Monthly Notices
of the
ROYAL ASTRONOMICAL SOCIETY

MNRAS **438,** 620–638 (2014)
Advance Access publication 2013 December 13

doi:10.1093/mnras/stt2231

Dynamical evolution of star-forming regions

Richard J. Parker,[1]★ Nicholas J. Wright,[2] Simon P. Goodwin[3] and Michael R. Meyer[1]

[1]*Institute for Astronomy, ETH Zürich, Wolfgang-Pauli-Strasse 27, CH-8093 Zürich, Switzerland*
[2]*Centre for Astrophysics Research, Science and Technology Research Institute, University of Hertfordshire, Hatfield AL10 9AB, UK*
[3]*Department of Physics and Astronomy, University of Sheffield, Sheffield S3 7RH, UK*

Accepted 2013 November 14. Received 2013 November 14; in original form 2013 September 5

ABSTRACT

We model the dynamical evolution of star-forming regions with a wide range of initial properties. We follow the evolution of the regions' substructure using the $\mathcal{Q}$-parameter, we search for dynamical mass segregation using the $\Lambda_{\rm MSR}$ technique, and we also quantify the evolution of local density around stars as a function of mass using the $\Sigma_{\rm LDR}$ method. The amount of dynamical mass segregation measured by $\Lambda_{\rm MSR}$ is generally only significant for subvirial and virialized, substructured regions – which usually evolve to form bound clusters. The $\Sigma_{\rm LDR}$ method shows that massive stars attain higher local densities than the median value in *all* regions, even those that are supervirial and evolve to form (unbound) associations. We also introduce the $\mathcal{Q} - \Sigma_{\rm LDR}$ plot, which describes the evolution of spatial structure as a function of mass-weighted local density in a star-forming region. Initially dense ($>$1000 stars pc^{-2}), bound regions always have $\mathcal{Q} > 1$, $\Sigma_{\rm LDR} > 2$ after 5 Myr, whereas dense unbound regions always have $\mathcal{Q} < 1$, $\Sigma_{\rm LDR} > 2$ after 5 Myr. Less dense regions ($<$100 stars pc^{-2}) do not usually exhibit $\Sigma_{\rm LDR} > 2$ values, and if relatively high local density around massive stars arises purely from dynamics, then the $\mathcal{Q} - \Sigma_{\rm LDR}$ plot can be used to estimate the initial density of a star-forming region.

Key words: methods: numerical – stars: formation – open clusters and associations: general.

1 INTRODUCTION

Understanding the earliest phases of the dynamical evolution of stars is important as their birth environments can impact planetary systems (through interactions with discs, or through encounters with young planetary systems), as well as stellar properties such as multiplicity. Star formation occurs most often in regions significantly denser than the field in which interactions may be common[1] (Lada & Lada 2003; Gieles & Portegies Zwart 2011; Kruijssen 2012). Only a small fraction (∼10 per cent, Lada & Lada 2003) of stars remain in bound (open) clusters after 10 Myr, and so the vast majority of young stars disperse rapidly into the field. It is interesting and important to know how and why most star-forming regions dissolve rapidly, and what encounters stars may have had before this dissolution. Understanding this may place in context the exoplanet properties of nearby field stars.

Recent results from the *Herschel* space telescope have shown that stars initially form in filamentary structures (e.g. André et al. 2010), which results in hierarchical spatial distributions in star-forming regions (Cartwright & Whitworth 2004; Sánchez & Alfaro 2009). However, observations of some young (∼1 Myr) clusters show them to be centrally concentrated, with smooth radial profiles (e.g. the Orion Nebular Cluster (ONC) and IC 348 – Hillenbrand & Hartmann 1998; Cartwright & Whitworth 2004). Numerical studies have shown that substructure can be erased on very short timescales (Scally & Clarke 2002; Goodwin & Whitworth 2004; Allison et al. 2010), consistent with the hypothesis that all star-forming regions form with substructure, and a certain fraction dynamically evolve to attain smooth, centrally concentrated profiles – i.e. bound clusters, whereas the remainder form unbound associations that rapidly dissolve (Kruijssen 2012; Parker & Meyer 2012).

If stars do form in substructured distributions, and this substructure is erased in some star-forming regions, then in principle it may be possible to compare observations of star clusters and associations at different ages and use measures of structure and kinematics to infer the past, and potentially future, (dynamical) evolution of the system.

As an example, the competitive accretion scenario of star formation (Zinnecker 1982; Bonnell et al. 2001; Bonnell, Bate & Vine 2003; Bonnell, Clark & Bate 2008) predicts that the most massive stars are overconcentrated at the centre of a region (primordial mass segregation). We would not expect a region to lose any primordial mass segregation due to dynamical evolution. Whilst mass segregation is observed in several clusters [e.g. the ONC; Hillenbrand & Hartmann 1998, Allison et al. 2009b; NGC 3603 (Pang et al. 2013)

★ E-mail: rparker@phys.ethz.ch

[1] The typical field stellar density is around 0.1 stars pc^{-3} (Korchagin et al. 2003) which is much lower than the densities of even loose associations, e.g. Taurus with roughly 5 stars pc^{-3}, and very much lower than clusters, e.g. the Orion nebula Cluster with around 5000 stars pc^{-3} (King et al. 2012a).

and Trumpler 14; Sana et al. 2010], it is not clear whether it is primordial (i.e. an outcome of the star formation process). Recently, Allison et al. (2009b, 2010) showed that mass segregation can occur dynamically on very short time-scales, negating the need for the most massive stars to form at the centre of the region, as previously thought (Bonnell & Davies 1998). Furthermore, observations of both high- and low-mass clusters (Berkeley 96 – Delgado et al. 2013; ρ Oph – Parker, Maschberger & Alves de Oliveira 2012) and associations (Taurus – Parker et al. 2011; Cyg OB2 – Wright et al. 2014) indicate that mass segregation is not always present.

Assuming mass segregation is not always primordial, a combined measure of the structure of a star-forming region, and the amount of mass segregation that can occur dynamically, could be a useful diagnostic for tracing the dynamical evolution (if any) of the region.

In this paper, we examine the dynamical evolution of N-body simulations of star-forming regions to ascertain how often, mass segregation occurs (and quantify the amount) as a function of the initial bulk motion (virial state) of stars, and the amount of initial substructure present in the region. We compare the evolution of spatial structure as measured by the $\mathcal{Q}$-parameter (Cartwright & Whitworth 2004; Cartwright & Whitworth 2009), the occurrence of mass segregation as measured by the $\Lambda_{\rm MSR}$ minimum spanning tree (MST) technique (Allison et al. 2009a), and we follow the evolution of the mass-weighted local density, $\Sigma - m$ (Maschberger & Clarke 2011).

We will refer to the young substructured star-forming complexes as *regions*, and only use the terminology 'cluster' or 'association' when describing the regions at later times when they have distinguishable morphologies.

The paper is organized as follows. We describe our N-body simulations in Section 2, in Section 3 we describe the algorithms used to quantify structure and mass segregation, we present our results in Section 4, we provide a discussion in Section 5 and we conclude in Section 6.

2 METHOD

The regions we simulate have either 1500 members, which corresponds to a mass of $\sim 10^3$ M$_\odot$, or 150 members, corresponding to a mass of $\sim 10^2$ M$_\odot$. For each set of initial conditions, we run an ensemble of 20 simulations, identical apart from the random number seed used to initialize the positions, masses and velocities of the stars.

Our model regions are set up as fractals; observations of young unevolved star-forming regions indicate a high level of substructure is present (i.e. they do not have a radially smooth profile, e.g. Cartwright & Whitworth 2004; Sánchez & Alfaro 2009; Schmeja 2011, and references therein). The fractal distribution provides a way of creating substructure on all scales. Note that we are not claiming that young star-forming regions are fractal (although they may be, e.g. Elmegreen & Elmegreen 2001), but the fractal distribution is a relatively simple method of setting up substructure, as the level of substructure is described by just one parameter, the fractal dimension, D. In three dimensions, $D = 1.6$ indicates a highly substructured region, and $D = 3.0$ is a roughly uniform sphere.

We set up the fractals according to the method in Goodwin & Whitworth (2004). This begins by defining a cube of side $N_{\rm div}$ (we adopt $N_{\rm div} = 2.0$ throughout), inside of which the fractal is built. A first-generation parent is placed at the centre of the cube, which then spawns $N_{\rm div}^3$ subcubes, each containing a first generation child at its centre. The fractal is then built by determining which of the children themselves become parents, and spawn their own offspring. This is determined by the fractal dimension, D, where the probability that the child becomes a parent is given by $N_{\rm div}^{(D-3)}$. For a lower fractal dimension fewer children mature and the final distribution contains more substructure. Any children that do not become parents in a given step are removed, along with all of their parents. A small amount of noise is then added to the positions of the remaining children, preventing the region from having a gridded appearance and the children become parents of the next generation. Each new parent then spawns $N_{\rm div}^3$ second-generation children in $N_{\rm div}^3$ sub-subcubes, with each second-generation child having a $N_{\rm div}^{(D-3)}$ probability of becoming a second generation parent. This process is repeated until there are substantially more children than required. The children are pruned to produce a sphere from the cube and are then randomly removed (so maintaining the fractal dimension) until the required number of children is left. These children then become stars in the model.

To determine the velocity structure of the cloud, children inherit their parent's velocity plus a random component that decreases with each generation of the fractal. The children of the first generation are given random velocities from a Gaussian of mean zero. Each new generation inherits their parent's velocity plus an extra random component that becomes smaller with each generation. This results in a velocity structure in which nearby stars have similar velocities, but distant stars can have very different velocities. The velocity of every star is scaled to obtain the desired virial ratio of the region. In one set of simulations, we do not correlate the velocities according to position, and simply choose them randomly from a Gaussian of mean zero before scaling to the global virial ratio.

We vary the initial global virial ratio, $\alpha_{\rm vir} = T/|\Omega|$, where T and $|\Omega|$ are the total kinetic energy and total potential energy of the stars, respectively. Note that a virial ratio of $\alpha_{\rm vir} = 0.5$ does *not* necessarily mean that the regions are in virial equilibrium. Because of the spatial and velocity substructure of the regions they are far from equilibrium and will undergo a violent relaxation phase to attempt to attain virial equilibrium and a smooth central profile (if they are bound). Because we have correlated the velocities of the stars on local scales, a substructured fractal with $\alpha_{\rm vir} = 0.5$ will violently relax in a similar way to a subvirial fractal. The main difference is that a subvirial fractal will collapse more quickly, and form a denser core, than a virial fractal (Allison et al. 2010). Similarly, a supervirial fractal will expand on a global scale, but the pockets of substructure will not be supervirial. For this reason, we introduce the following terminology: a globally subvirial fractal ($\alpha_{\rm vir} = 0.3$) is 'cool' because the stars are moving slowly with respect to their 'equilibrium' velocities, a globally virial fractal ($\alpha_{\rm vir} = 0.5$) is 'tepid' because the stars are still able to interact in the substructure and it is bound, and a globally supervirial fractal ($\alpha_{\rm vir} = 1.5$) is 'hot' and unbound.

The regions are set up with fractal dimensions of $D = 1.6$ (very clumpy), $D = 2.0$ and $D = 3.0$ (a roughly uniform sphere), in order to investigate the full parameter space. We reiterate that these initial conditions are based on observations of star-forming regions, which appear to be filamentary (e.g. André et al. 2010) and form stars with a hierarchical distribution (Elmegreen & Elmegreen 2001). This substructured distribution of stars is also consistent with the outcome of hydrodynamical simulations of star formation (e.g. Schmeja & Klessen 2006; Bate 2012; Dale, Ercolano & Bonnell 2012, 2013; Girichidis et al. 2012).

The regions contain 1500 or 150 stars each, have initial radii of 1 pc with no primordial binaries or gas potential. We draw stellar masses from the recent fit to the field initial mass function (IMF)

by Maschberger (2013) which has a probability density function of the form:

$$p(m) \propto \left(\frac{m}{\mu}\right)^{-\alpha} \left(1 + \left(\frac{m}{\mu}\right)^{1-\alpha}\right)^{-\beta}. \quad (1)$$

Equation (1) essentially combines the log-normal approximation for the IMF derived by Chabrier (2003, 2005) with the Salpeter (1955) power-law slope for stars with mass $>1\,\mathrm{M}_\odot$. Here, $\mu = 0.2\,\mathrm{M}_\odot$ is the average stellar mass, $\alpha = 2.3$ is the Salpeter power-law exponent for higher mass stars, and $\beta = 1.4$ is the power-law exponent to describe the slope of the IMF for low-mass objects (which also deviates from the log-normal form; Bastian, Covey & Meyer 2010). Finally, we sample from this IMF within the mass range $m_{\rm low} = 0.01\,\mathrm{M}_\odot$ to $m_{\rm up} = 50\,\mathrm{M}_\odot$.

It is worth noting that the *average global* surface and volume densities of all $N = 1500$ regions are very similar to each other (1500 stars in a 1 pc radius sphere), and similarly for the $N = 150$ star regions. However, the *average* local surface and volume densities vary by several orders of magnitude depending on the fractal dimension (degree of substructure). Highly substructured regions have their stars concentrated in local 'pockets' and have a filling factor much less than unity (to some degree this is the definition of a fractal). Thus, their local densities in these pockets may be considerable.

We run the simulations for 10 Myr using the KIRA integrator in the STARLAB package (Portegies Zwart et al. 1999, 2001). We do not include stellar evolution in the simulations. A summary of the simulation parameter space is given in Table 1.

Table 1. A summary of the different star-forming region properties adopted for the simulations. The values in the columns are: the number of stars in each region ($N_{\rm stars}$), the typical mass of this region ($M_{\rm region}$), the initial *global* virial ratio of the region ($\alpha_{\rm vir}$), the initial fractal dimension (D) and whether or not the stellar velocities are correlated by distance.

$N_{\rm stars}$	$M_{\rm region}$	$\alpha_{\rm vir}$	D	Correlated velocities?
1500	$\sim 10^3\,\mathrm{M}_\odot$	0.3	1.6	yes
1500	$\sim 10^3\,\mathrm{M}_\odot$	0.3	2.0	yes
1500	$\sim 10^3\,\mathrm{M}_\odot$	0.3	3.0	yes
1500	$\sim 10^3\,\mathrm{M}_\odot$	0.5	1.6	yes
1500	$\sim 10^3\,\mathrm{M}_\odot$	0.5	2.0	yes
1500	$\sim 10^3\,\mathrm{M}_\odot$	0.5	3.0	yes
1500	$\sim 10^3\,\mathrm{M}_\odot$	1.5	1.6	yes
1500	$\sim 10^3\,\mathrm{M}_\odot$	1.5	2.0	yes
1500	$\sim 10^3\,\mathrm{M}_\odot$	1.5	3.0	yes
150	$\sim 10^2\,\mathrm{M}_\odot$	0.3	1.6	yes
150	$\sim 10^2\,\mathrm{M}_\odot$	0.3	2.0	yes
150	$\sim 10^2\,\mathrm{M}_\odot$	0.3	3.0	yes
150	$\sim 10^2\,\mathrm{M}_\odot$	0.5	1.6	yes
150	$\sim 10^2\,\mathrm{M}_\odot$	0.5	2.0	yes
150	$\sim 10^2\,\mathrm{M}_\odot$	0.5	3.0	yes
150	$\sim 10^2\,\mathrm{M}_\odot$	1.5	1.6	yes
150	$\sim 10^2\,\mathrm{M}_\odot$	1.5	2.0	yes
150	$\sim 10^2\,\mathrm{M}_\odot$	1.5	3.0	yes
1500	$\sim 10^3\,\mathrm{M}_\odot$	1.5	1.6	no

3 QUANTIFYING SPATIAL STRUCTURE AND MASS SEGREGATION

3.1 Measuring spatial structure

We determine the amount of structure in a star-forming region by measuring the $\mathcal{Q}$-parameter. The $\mathcal{Q}$-parameter was pioneered by Cartwright & Whitworth (2004); Cartwright & Whitworth (2009); Cartwright (2009) and combines the normalized mean edge length of the minimum spanning tree of all the stars in the region, $\bar{m}$, with the normalized correlation length between all stars in the region, $\bar{s}$. The level of substructure is determined by the following equation:

$$\mathcal{Q} = \frac{\bar{m}}{\bar{s}}. \quad (2)$$

A substructured association or region has $\mathcal{Q} < 0.8$, whereas a smooth, centrally concentrated cluster has $\mathcal{Q} > 0.8$. The $\mathcal{Q}$-parameter has the advantage of being independent of the density of the star-forming region, and purely measures the level of substructure present. The original formulation of the $\mathcal{Q}$-parameter assumes the region is spherical, but can be modified to take into account the effects of elongation (Bastian et al. 2009; Cartwright & Whitworth 2009).

3.2 Measuring mass segregation

Mass segregation is a rather difficult thing to define. It is usually considered in the case of bound (spherical) clusters where a degree of energy equipartition (primordial, dynamical or both) results in the most massive stars preferentially located in the cluster centre.

However, here we take a more general definition of mass segregation applicable to substructured regions and associations, as well as clusters. One way of viewing 'mass segregation' is that the massive stars are *closer to each other* than would be expected of random stars (this is what is measured by the $\Lambda_{\rm MSR}$-parameter, see below). Another view is that the massive stars are in *locally denser regions* than would be expected of a typical star (this is what is measured by the $\Sigma - m$ method, again see below for details).

Note that there are many other ways of defining mass segregation. For example, one can choose a cluster centre and measure the mass function as a function of radial distance (Gouliermis et al. 2004; Sabbi et al. 2008), use the mean square (*Spitzer*) radius of the cluster as a diagnostic for comparing stars with different mass ranges (Gouliermis, de Grijs & Xin 2009) or determine the distance of the most massive star(s) from the cluster centre compared to the average distance of low-mass stars to the cluster centre (Kirk & Myers 2011). It is also possible to quantify differences in luminosity between the centre and outskirts of a cluster (e.g. Carpenter et al. 1997).

However, it is important to note that the $\Lambda_{\rm MSR}$ and the $\Sigma - m$ methods have the significant advantage over other methods in that they do not require the determination of a 'centre' in a region, which is crucial for analysing highly substructured regions.

3.2.1 *The $\Lambda_{\rm MSR}$ mass segregation ratio*

In order to quantify the amount of mass segregation present in a region, we first use the $\Lambda_{\rm MSR}$ method, introduced by Allison et al. (2009a). This constructs an MST between a chosen subset of stars

and then compares this MST to the average MST length of many random subsets.

The MST of a set of points is the path connecting all the points via the shortest possible path length but which contains no closed loops (e.g. Prim 1957; Cartwright & Whitworth 2004).

We use the algorithm of Prim (1957) to construct MSTs in our data set. We first make an ordered list of the separations between all possible pairs of stars. Stars are then connected together in 'nodes', starting with the shortest separations and proceeding through the list in order of increasing separation, forming new nodes if the formation of the node does not result in a closed loop.

We find the MST of the $N_{\rm MST}$ stars in the chosen subset and compare this to the MST of sets of $N_{\rm MST}$ random stars in the region. If the length of the MST of the chosen subset is shorter than the average length of the MSTs for the random stars then the subset has a more concentrated distribution and is said to be mass segregated. Conversely, if the MST length of the chosen subset is longer than the average MST length, then the subset has a less concentrated distribution, and is said to be inversely mass segregated (see e.g. Parker et al. 2011). Alternatively, if the MST length of the chosen subset is equal to the random MST length, we can conclude that no mass segregation is present.

By taking the ratio of the average (mean) random MST length to the subset MST length, a quantitative measure of the degree of mass segregation (normal or inverse) can be obtained. We first determine the subset MST length, $l_{\rm subset}$. We then determine the average length of sets of $N_{\rm MST}$ random stars each time, $\langle l_{\rm average}\rangle$. There is a dispersion associated with the average length of random MSTs, which is roughly Gaussian and can be quantified as the standard deviation of the lengths $\langle l_{\rm average}\rangle \pm \sigma_{\rm average}$. However, we conservatively estimate the lower (upper) uncertainty as the MST length which lies 1/6 (5/6) of the way through an ordered list of all the random lengths (corresponding to a 66 per cent deviation from the median value, $\langle l_{\rm average}\rangle$). This determination prevents a single outlying object from heavily influencing the uncertainty. We can now define the 'mass segregation ratio' ($\Lambda_{\rm MSR}$) as the ratio between the average random MST path length and that of a chosen subset, or mass range of objects:

$$\Lambda_{\rm MSR} = \frac{\langle l_{\rm average}\rangle}{l_{\rm subset}}{}^{+\sigma_{5/6}/l_{\rm subset}}_{-\sigma_{1/6}/l_{\rm subset}}. \quad (3)$$

A $\Lambda_{\rm MSR}$ of $\sim$1 shows that the stars in the chosen subset are distributed in the same way as all the other stars, whereas $\Lambda_{\rm MSR} > 1$ indicates mass segregation and $\Lambda_{\rm MSR} < 1$ indicates inverse mass segregation, i.e. the chosen subset is more sparsely distributed than the other stars.

There are several subtle variations of $\Lambda_{\rm MSR}$. Olczak, Spurzem & Henning (2011) propose using the geometric mean to reduce the spread in uncertainties, and Maschberger & Clarke (2011) propose using the median MST length to reduce the effects of outliers from influencing the results. However, in the subsequent analysis we will adopt the original $\Lambda_{\rm MSR}$ from Allison.

3.3 The $\Sigma - m$ method and the $\Sigma_{\rm LDR}$ local density ratio

Recently, Maschberger & Clarke (2011) proposed a method to analyse mass segregation which measures the distribution of local stellar surface density, Σ, as a function of stellar mass. We calculate the local stellar surface density following the prescription of Casertano & Hut (1985), modified to account for the analysis in projection. For an individual star, the local stellar surface density is given by

$$\Sigma = \frac{N-1}{\pi r_N^2}, \quad (4)$$

where r_N is the distance to the $N^{\rm th}$ nearest neighbouring star (we adopt $N = 10$ throughout this work).

If there is mass segregation, massive stars are concentrated in the central, dense regions and thus should have higher values of Σ. This can be seen in a plot of Σ versus mass, showing all stars and highlighting outliers. Trends in the $\Sigma - m$ plot can be shown by the moving average (or median) of a subset, $\tilde{\Sigma}_{\rm subset}$, compared to the average (median) of the whole sample, $\tilde{\Sigma}_{\rm all}$. The signature of mass segregation is then $\tilde{\Sigma}_{\rm subset} > \tilde{\Sigma}_{\rm all}$, and of inverse mass segregation $\tilde{\Sigma}_{\rm subset} < \tilde{\Sigma}_{\rm all}$. The statistical significance of mass segregation can be established with a two-sample Kolmogorov–Smirnov (KS) test of the Σ values of the subset against the Σ values of the rest.

Note that the $\Sigma - m$ method shares similarities with the two-dimensional convex hull method proposed by Moeckel & Bonnell (2009b), in that as well as measuring the degree of mass segregation, it also provides information on the density within a region.

Whilst this method has the advantage of not being biased by outliers (see the discussion in Maschberger & Clarke 2011), it does lead to the artificial effect of placing each (massive) star in its own bin (defined by the local density of that star), and does not always reflect the *spatial* distribution of a particular subset of stars. What it does effectively measure is the *local density* distribution of a subset, which we will see in Section 4 is not necessarily the spatial distribution.

In this paper, we will divide $\tilde{\Sigma}_{\rm subset}$ by $\tilde{\Sigma}_{\rm all}$ to define a 'local density ratio', $\Sigma_{\rm LDR}$ (see also Kupper et al. 2011):

$$\Sigma_{\rm LDR} = \frac{\tilde{\Sigma}_{\rm subset}}{\tilde{\Sigma}_{\rm all}}. \quad (5)$$

The significance of this measure of the local density of a subset of stars compared to the cluster will still be defined by the KS test between the Σ values of the subset against the Σ values of the rest. We will detail the number of stars used to determine $\tilde{\Sigma}_{\rm subset}$ in the following sections of the paper.

The differences between $\Lambda_{\rm MSR}$ and $\Sigma_{\rm LDR}$ might seem subtle, but (as we shall see) become important. The $\Lambda_{\rm MSR}$ method measures the collective concentration of massive stars (i.e. are they close to each other?). The $\Sigma_{\rm LDR}$ method measures the relative local densities of massive stars (i.e. are they in dense regions?), but does not consider how close the massive stars are to each other. Therefore, it would be quite possible (and we find it so) to have significant 'mass segregation' found by one method but not the other. For this reason, we do not refer to $\Sigma - m$ as measuring 'mass segregation' in the remainder of the paper.

4 RESULTS

In this section, we first examine the evolution of typical examples of a substructured, subvirial (cool) star-forming region and a substructured, supervirial (warm) region, before comparing the average evolution of all of the models in our chosen parameter space. We use the $\Lambda_{\rm MSR}$ measure of mass segregation, the $\Sigma_{\rm LDR}$ measure of local density, as well as a measure of the spatial structure of the region ($\mathcal{Q}$) described in Section 3, and follow the evolution of these quantities over time.

4.1 Evolution of a substructured, subvirial region

In Fig. 1, we show the evolution of a 'typical'[2] $N = 1500$ stars, subvirial ($\alpha_{\rm vir} = 0.3$), substructured ($D = 1.6$) region. In panels (a)–(c), we show the morphology at 0, 5 and 10 Myr, respectively. This region undergoes violent relaxation and collapses to form a bound, spherical cluster. The most massive stars (shown by the red triangles) are randomly placed in the fractal initially but after 5 Myr they are all in the cluster centre and have dynamically mass segregated.

As the cluster relaxes, the most massive stars interact with each other, often forming unstable hierarchical multiple systems (Allison & Goodwin 2011) – indeed, the binary fraction of O-type stars in the simulation rises from zero to ∼70 per cent after 10 Myr. The formation of massive star binaries can in some cases destroy the cluster, as e.g. a 30 $M_\odot$–30 $M_\odot$ binary with 100 au semimajor axis has a binding energy comparable to that of the whole cluster (10^{41} J), and this process is apparent after 10 Myr (panel c).

We can examine this behaviour using the $\Lambda_{\rm MSR}$ measure of mass segregation. In panel (d), the mass segregation ratio as a function of the number of stars in the MST, $N_{\rm MST}$ is shown at 0 Myr (i.e. before any dynamical evolution has occurred). The region rapidly mass segregates due to its initial subvirial velocities and high level of substructure (as demonstrated by Allison et al. 2010), with significant mass segregation down to the 40th most massive star after 5 Myr (panel e). For example, if we focus on the a subset of stars more massive than the $N_{\rm MST} = 10^{\rm th}$ most massive star, the cluster has a mass segregation ratio $\Lambda_{\rm MSR} = 7.6^{+5.1}_{-2.9}$. However, as the higher order massive star multiple system in the centre decays (see Allison & Goodwin 2011) the amount of mass segregation (as measured by $\Lambda_{\rm MSR}$) decreases to the point at which is not significant at 10 Myr (panel f).

In panel (g), we show the local surface density of every star in the region as a function of the star's mass (the grey points). The median stellar surface density for the entire region is indicated by the blue dashed line in Fig. 1(g). Initially, the median surface density for all stars in the region is $\tilde{\Sigma}_{\rm all} = 7187$ stars pc^{-2}, whereas the 10 most massive stars have a median surface density $\tilde{\Sigma}_{10} = 5829$ stars pc^{-2} as shown by the solid red line. This difference, however, is not significant – a two-dimensional KS test returns a p-value of 0.57 that the two subsets share the same parent distribution. However, after 5 Myr (panel h) the most massive stars have a median surface density of $\tilde{\Sigma}_{10} = 708$ stars pc^{-2} compared to the cluster median value of $\tilde{\Sigma}_{\rm all} = 90$ stars pc^{-2}. Now the KS test between these two subsets returns a p-value of $<10^{-5}$, indicating that the massive stars are in areas of significantly higher local density than the average stars in the region. After 10 Myr, the 10 most massive stars again have a higher surface density $\tilde{\Sigma}_{10} = 87$ stars pc^{-2}, whereas the median surface density for the whole cluster is $\tilde{\Sigma}_{\rm all} = 29$ stars pc^{-2}.

We show the full evolution of $\Lambda_{\rm MSR}$ in Fig. 1(j). The value of $\Lambda_{\rm MSR}$ for the 10 most massive stars is shown by the solid line (with error bars), and $\Lambda_{\rm MSR}$ for the 20 and 50 most massive stars is shown by the dashed and dot–dashed lines, respectively. We plot $\Lambda_{\rm MSR} = 1$, i.e. no mass segregation, shown by the horizontal red line. The region has dynamically mass segregated on a significant level after 1.5 Myr, and the value of $\Lambda_{\rm MSR}$ reaches a maximum of $\Lambda_{\rm MSR} = 11.2^{+6.2}_{-4.3}$ after 4.3 Myr.

[2] By 'typical' we mean that it shows the basic dynamics that occur in such a system, as we shall describe later different realizations of statistically the same initial conditions can result in very different behaviour (see Allison et al. 2010).

In Fig. 1(k), we show the evolution of the surface density of the 10 most massive stars divided by the median surface density (the $\Sigma_{\rm LDR}$ local density ratio, $\Sigma_{\rm LDR} = \tilde{\Sigma}_{10}/\tilde{\Sigma}_{\rm all}$) in the region as a function of time. We plot a filled red circle at times when the difference between the most massive stars and the whole region is not significant (in this case only the first few snapshots in the N-body simulation). We plot $\Sigma_{\rm LDR} = 1$, (i.e. no difference in local density as a function of mass) shown by the horizontal red line. The $\Sigma_{\rm LDR}$ ratio quickly becomes significantly higher than unity, and is above 5 for the majority of the cluster's lifetime.

Finally, we plot the evolution of the spatial structure (as measured by the $\mathcal{Q}$–parameter) in Fig. 1(l). The boundary between substructured and centrally concentrated morphologies ($\mathcal{Q} = 0.8$) is shown by the grey dashed line. The initial substructure is rapidly erased (as demonstrated in Goodwin & Whitworth 2004; Parker & Meyer 2012) and the region becomes a smooth, centrally concentrated cluster after only 1 Myr (on a similar time-scale to the mass segregation).

4.2 Evolution of a substructured, supervirial region

In Fig. 2, we show the evolution of a 'typical' $N = 1500$ stars, supervirial ($\alpha_{\rm vir} = 1.5$), substructured ($D = 1.6$) star-forming region. As in Fig. 1, in panels (a)–(c) we show the morphology at 0, 5 and 10 Myr, respectively. The most massive stars (shown by the red triangles) are initially randomly placed in the substructured fractal. The global motion of the region causes it to expand and after 5 Myr two distinct subclusters have formed, separated by a distance of ∼20 pc. However, there are also stars in between, and the region has evolved into an association-like complex. The association expands further until the simulation end-time at 10 Myr.

We measure $\Lambda_{\rm MSR}$ for this region; in panel (d) the mass segregation ratio as a function of the number of stars in the MST, $N_{\rm MST}$ is shown at 0 Myr (i.e. before any dynamical evolution has occurred). Unlike the subvirial, collapsing fractal shown in Fig. 1, this supervirial, expanding fractal does not show any evidence of dynamical mass segregation at 5 or 10 Myr (panels e and f, respectively). This is unsurprising as the massive stars have no opportunity to become concentrated together.

Note that this is not simply due to the inclusion of 'outliers' in the determination of $\Lambda_{\rm MSR}$; varying the number of stars in the MST does not change the result.

In panel (g), we show the local surface density of every star in the region as a function of the star's mass (the grey points). The median stellar surface density for the entire region is indicated by the blue dashed line in Fig. 2(g). Initially, the median surface density is $\tilde{\Sigma}_{\rm all} = 5052$ stars pc^{-2}, whereas the 10 most massive stars have a median surface density of $\tilde{\Sigma}_{10} = 4356$ stars pc^{-2} as shown by the solid red line. This difference is not significant – a two-dimensional KS test returns a p-value of 0.58 that the two subsets share the same parent distribution. However, the region massive stars in the region subsequently attain much higher local densities than the average star in the region. After 5 Myr (panel h), the most massive stars have a median surface density of $\tilde{\Sigma}_{10} = 277$ stars pc^{-2} compared to the region median value of $\tilde{\Sigma}_{\rm all} = 15$ stars pc^{-2}. Now the KS test between these two subsets returns a p-value of $<10^{-3}$, indicating a significant difference. After 10 Myr the 10 most massive stars again have a higher surface density $\tilde{\Sigma}_{10} = 92$ stars pc^{-2}, whereas the median surface density for the whole association is $\tilde{\Sigma}_{\rm all} = 5$ stars pc^{-2}.

The evolution of $\Lambda_{\rm MSR}$ for the duration of the simulation is shown in Fig. 2(j). The value of $\Lambda_{\rm MSR}$ for the 10 most massive stars is shown by the solid line (with error bars), and $\Lambda_{\rm MSR}$ for the 20 and

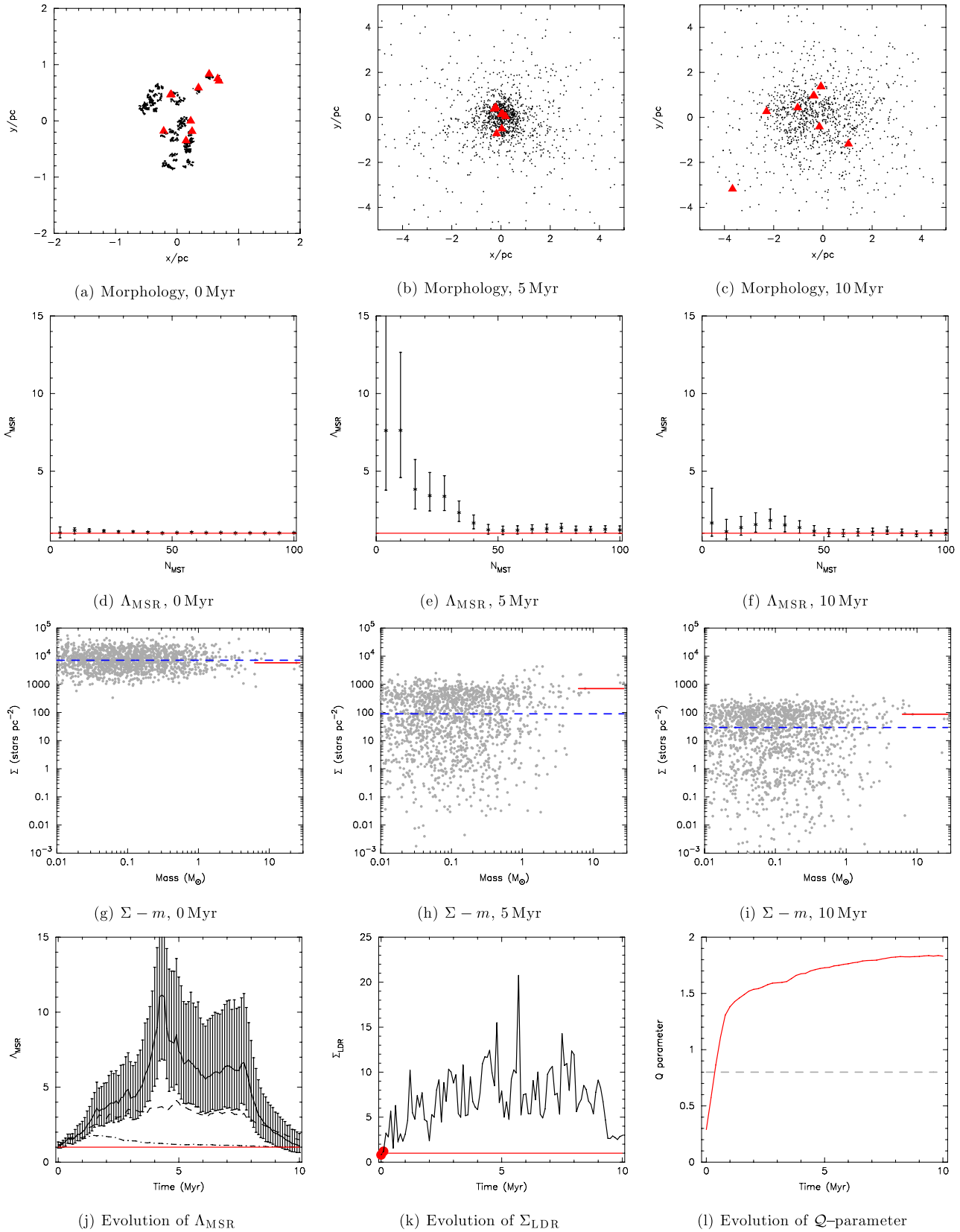

(a) Morphology, 0 Myr (b) Morphology, 5 Myr (c) Morphology, 10 Myr

(d) $\Lambda_{\rm MSR}$, 0 Myr (e) $\Lambda_{\rm MSR}$, 5 Myr (f) $\Lambda_{\rm MSR}$, 10 Myr

(g) $\Sigma - m$, 0 Myr (h) $\Sigma - m$, 5 Myr (i) $\Sigma - m$, 10 Myr

(j) Evolution of $\Lambda_{\rm MSR}$ (k) Evolution of $\Sigma_{\rm LDR}$ (l) Evolution of $\mathcal{Q}$–parameter

Figure 1. Evolution of a subvirial ($\alpha_{\rm vir} = 0.3$), substructured star-forming region ($D = 1.6$) with $N = 1500$ stars. We show the morphology at 0, 5 and 10 Myr (a)–(c), the mass segregation ratio, $\Lambda_{\rm MSR}$ of the $N_{\rm MST}$ most massive stars at 0, 5 and 10 Myr (d)–(f), and the surface density as a function of stellar mass, $\Sigma - m$ (g)–(i) at 0, 5 and 10 Myr. We also show the evolution of $\Lambda_{\rm MSR}$ in panel (j) – the solid, dashed and dot–dashed lines are the values of $\Lambda_{\rm MSR}$ for the 10, 20 and 50 most massive stars, respectively; the ratio of the surface density of the 10 most massive stars to the median surface density of all stars in the region ($\Sigma_{\rm LDR} = \bar{\Sigma}_{10}/\bar{\Sigma}_{\rm all}$ – panel k) and the evolution of the $\mathcal{Q}$–parameter (panel l), with time.

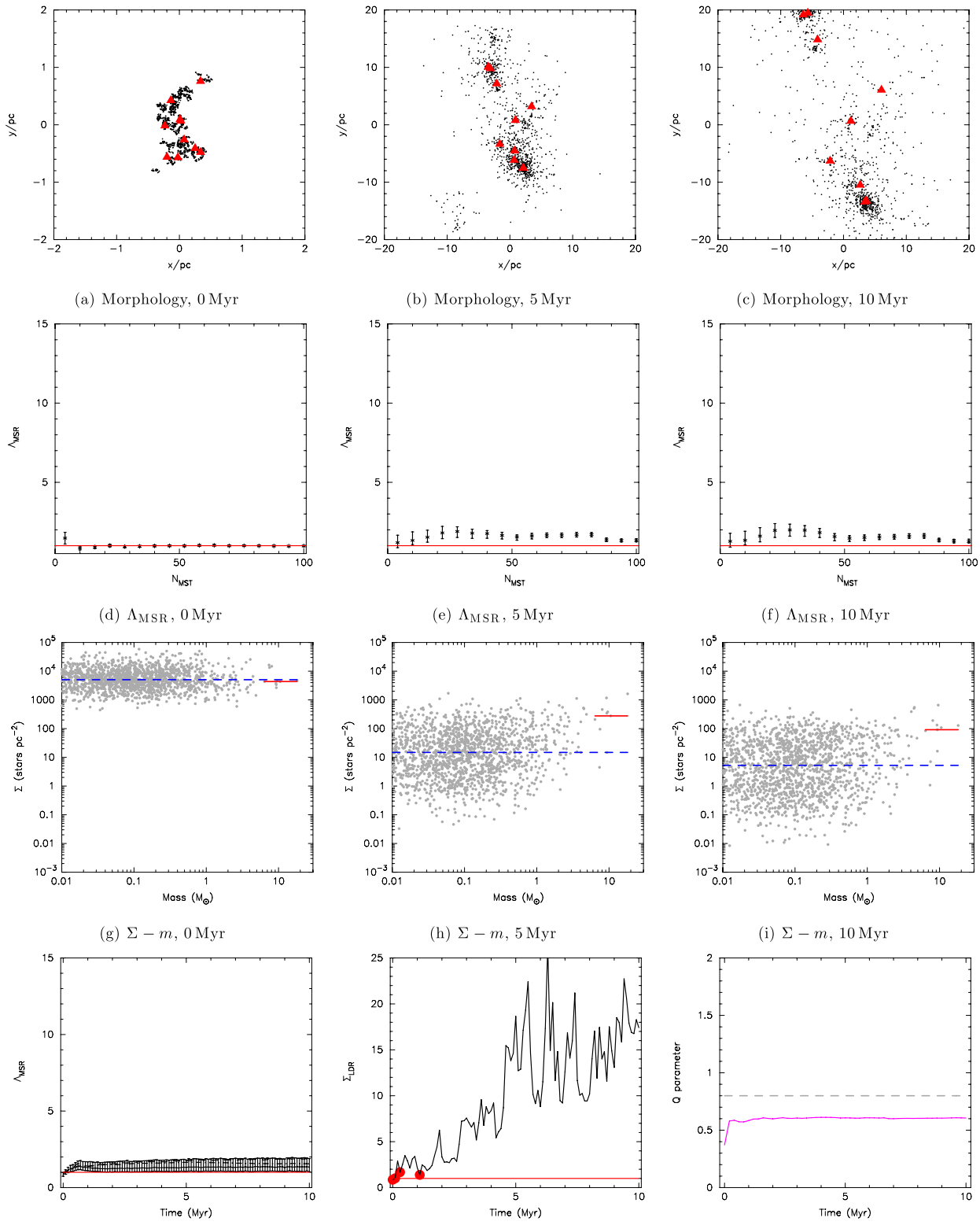

(a) Morphology, 0 Myr (b) Morphology, 5 Myr (c) Morphology, 10 Myr

(d) $\Lambda_{\rm MSR}$, 0 Myr (e) $\Lambda_{\rm MSR}$, 5 Myr (f) $\Lambda_{\rm MSR}$, 10 Myr

(g) $\Sigma - m$, 0 Myr (h) $\Sigma - m$, 5 Myr (i) $\Sigma - m$, 10 Myr

(j) Evolution of $\Lambda_{\rm MSR}$ (k) Evolution of $\Sigma_{\rm LDR}$ (l) Evolution of $\mathcal{Q}$–parameter

Figure 2. Evolution of a supervirial ($\alpha_{\rm vir} = 1.5$), substructured star-forming region ($D = 1.6$) with $N = 1500$ stars. We show the morphology at 0, 5 and 10 Myr (a–c), the mass segregation ratio, $\Lambda_{\rm MSR}$ of the $N_{\rm MST}$ most massive stars at 0, 5 and 10 Myr (d–f), and the surface density as a function of stellar mass, $\Sigma - m$ (g–i) at 0, 5 and 10 Myr. We also show the evolution of $\Lambda_{\rm MSR}$ in panel (j) – the solid, dashed and dot–dashed lines are the values of $\Lambda_{\rm MSR}$ for the 10, 20 and 50 most massive stars, respectively; the ratio of the surface density of the 10 most massive stars to the median surface density of all stars in the region ($\Sigma_{\rm LDR} = \bar{\Sigma}_{10}/\bar{\Sigma}_{\rm all}$ – panel k) and the evolution of the $\mathcal{Q}$–parameter (panel l), with time.

50 most massive stars is shown by the dashed and dot–dashed lines, respectively. We plot $\Lambda_{\rm MSR} = 1$, i.e. no mass segregation, shown by the horizontal red line. It is apparent that the region does not show any mass segregation according to the definition of $\Lambda_{\rm MSR}$.

Conversely, the strong difference in the density distribution of the massive stars from the $\Sigma - m$ measure at 5 Myr (Fig. 2h) and 10 Myr (Fig. 2i) is apparent throughout the lifetime of the region. In Fig. 2(k), we show the evolution of the surface density of the 10 most massive stars divided by the surface density for the whole region ($\Sigma_{\rm LDR} = \tilde{\Sigma}_{10}/\tilde{\Sigma}_{\rm all}$) as a function of time. We show $\Sigma_{\rm LDR} = 1$, i.e. no difference in local density as a function of mass, by the horizontal red line. We plot a filled red circle at times when the difference between the most massive stars and every star in the region is not significant – which occurs at 0, 0.25 and 1.2 Myr. However, after this time the $\Sigma_{\rm LDR}$ ratio rises steadily during the remainder of the simulation.

The very different behaviours of $\Lambda_{\rm MSR}$ and $\Sigma_{\rm LDR}$ are because they trace different physical processes. $\Lambda_{\rm MSR}$ is tracing the relative closeness of the massive stars *to each other*. As the region expands, the massive stars approximately keep their initial relative distributions as there is no way that they can know about each other, hence $\Lambda_{\rm MSR}$ remains low. But $\Sigma_{\rm LDR}$ measures the local density of stars around each *individual* massive star. The increase in $\Sigma_{\rm LDR}$ tells us that whilst the massive stars know nothing about each other, they do act as a potential well for nearby low-mass stars to fall into, increasing the local density around them. $\Sigma_{\rm LDR}$ continues to increase as the massive stars build larger and larger 'retinues' of low-mass stars.

We plot the evolution of structure in this model (as measured by the $\mathcal{Q}$–parameter) in Fig. 2(l). The boundary between substructured and centrally concentrated morphologies ($\mathcal{Q} = 0.8$) is shown by the grey dashed line. The $\mathcal{Q}$-parameter rises rapidly from its original value of $\mathcal{Q} = 0.4$, but then remains at $\mathcal{Q} \simeq 0.6$ for the remainder of the simulation, indicating that the region is still substructured (as is evident in the morphology at 5 and 10 Myr (panels b and c, respectively). In the initial rise in $\mathcal{Q}$ is due to the dispersion of some local substructure, and mergers between some nearby regions of substructure.

4.3 Evolution of all regions

The models presented in Figs 1 and 2 were chosen as 'typical' examples from each suite of 20 initially *statistically* identical simulations. However, the dynamical evolution of clusters can be highly stochastic; Allison et al. (2010) showed that statistically identical initial conditions can result in very different evolution. With this in mind, it is essential to consider ensembles of simulations in order to examine the spread in evolution and outcomes.

4.3.1 *Evolution of the $\mathcal{Q}$-parameter*

We first consider the evolution of spatial structure, as measured by the $\mathcal{Q}$-parameter, in each of our nine suites of simulations ($N = 1500$ stars and $\alpha_{\rm vir} = 0.3$, 0.5, 1.5 paired with $D = 1.6$, 2.0, 3.0). In Fig. 3, we show the evolution of the $\mathcal{Q}$-parameter with time – the boundary between substructured and radially smooth clusters ($\mathcal{Q} = 0.8$) is shown by the dashed grey line. For clarity, we only show the first 10 simulations (rather than all 20), but later we will include the $\mathcal{Q}$-parameter from every simulation at specific times in Figs 6 and 7.

If we compare the cool regions (Figs 3a–c) with the tepid regions (Figs 3d–f), we see that substructure is erased on similar time-scales (i.e. $\mathcal{Q}$ becomes greater than 0.8 within the first 1 Myr). This shows the erasure of substructure on roughly a crossing time (see e.g. Goodwin & Whitworth 2004).

On average, the cool regions (top row panels a–c) become more centrally concentrated (i.e. they reach higher values of $\mathcal{Q}$) than the tepid regions (middle row, panels d–f). Similarly, regions with more initial substructure ($D = 1.6$ in panels a and d in the first column) become more centrally concentrated than initially fairly smooth regions ($D = 3.0$ in panels c and f in the third column). This is due to the lower energy of the cool regions, and greater potential energy stored in substructure in the clumpy regions allowing a deeper collapse (e.g. Allison et al. 2009b, 2010).

However, the spread between the 10 simulations with identical initial conditions is so large that it becomes difficult to distinguish between different initial fractal dimensions and virial ratios for any *individual* region using the $\mathcal{Q}$-parameter alone. All sets of initial conditions can produce systems with $\mathcal{Q} = 1.5$ after 10 Myr. But it is worth noting that values of $\mathcal{Q}$ near 2 are only formed from initially substructured initial conditions.

In contrast, all supervirial regions ($\alpha_{\rm vir} = 1.5$ on the bottom row, panels g–i) keep a low ($\leq$0.8) value of the $\mathcal{Q}$-parameter. In the case of initially substructured regions (panels g and h), this is because they expand and so are unable to erase their substructure (see Goodwin & Whitworth 2004).

Interestingly, several of the initially smooth ($D = 3.0$, panel i) regions develop substructure as they expand ($\mathcal{Q}$ falls). This is due to the way the initial conditions are implemented. Whilst the $D = 3.0$ systems are roughly a uniform density sphere they do contain velocity substructure inherited from their 'parents' (see Section 2). However, unless one believes that fairly uniform density regions would form with uncorrelated and well mixed velocities, this may well not be particularly unphysical.

4.3.2 *Evolution of $\Lambda_{\rm MSR}$*

In Fig. 4, we show the evolution of the $\Lambda_{\rm MSR}$ (always for the tenth most massive star) mass segregation ratio for all nine ensembles of initial conditions in our parameter space (again, $N = 1500$ stars and $\alpha_{\rm vir} = 0.3$, 0.5, 1.5 paired with $D = 1.6$, 2.0, 3.0).

Unlike in Fig. 3 above, the results are far too variable to plot each individual simulation in an ensemble without producing a completely unreadable figure. Instead, at each time we plot the median value of $\Lambda_{\rm MSR}$ in each ensemble by the black cross. The range covered by half of the simulations (i.e. between the 25 and 75 percentiles) are shown by the black bars (these are *not* error bars in the conventional sense). The whole range covered at any time is indicated by the grey bars.

It should be noted that the evolution of any single system is not a simple passage through this range. Systems with high-$\Lambda_{\rm MSR}$ at 1 Myr may have either high- or low-$\Lambda_{\rm MSR}$ by 10 Myr and vice-versa (see Allison et al. 2010 for a fuller investigation of the evolution of $\Lambda_{\rm MSR}$).

Unsurprisingly, the bottom row of Fig. 4 for hot regions shows no sign of mass segregation in $\Lambda_{\rm MSR}$ no matter what the initial level of substructure. $\Lambda_{\rm MSR}$ starts at roughly unity and remains there as the regions expand giving the massive stars no chance to concentrate in any one place (values of about 2 are achievable if by chance two or three massive stars are initially close to one another).

Cool and tepid regions show a wide variety in the evolution of $\Lambda_{\rm MSR}$. Because of the initial conditions every region starts at $\Lambda_{\rm MSR} = 1$. As found by Allison et al. (2010), the evolution of these regions can be very stochastic. Generally, regions will relax and

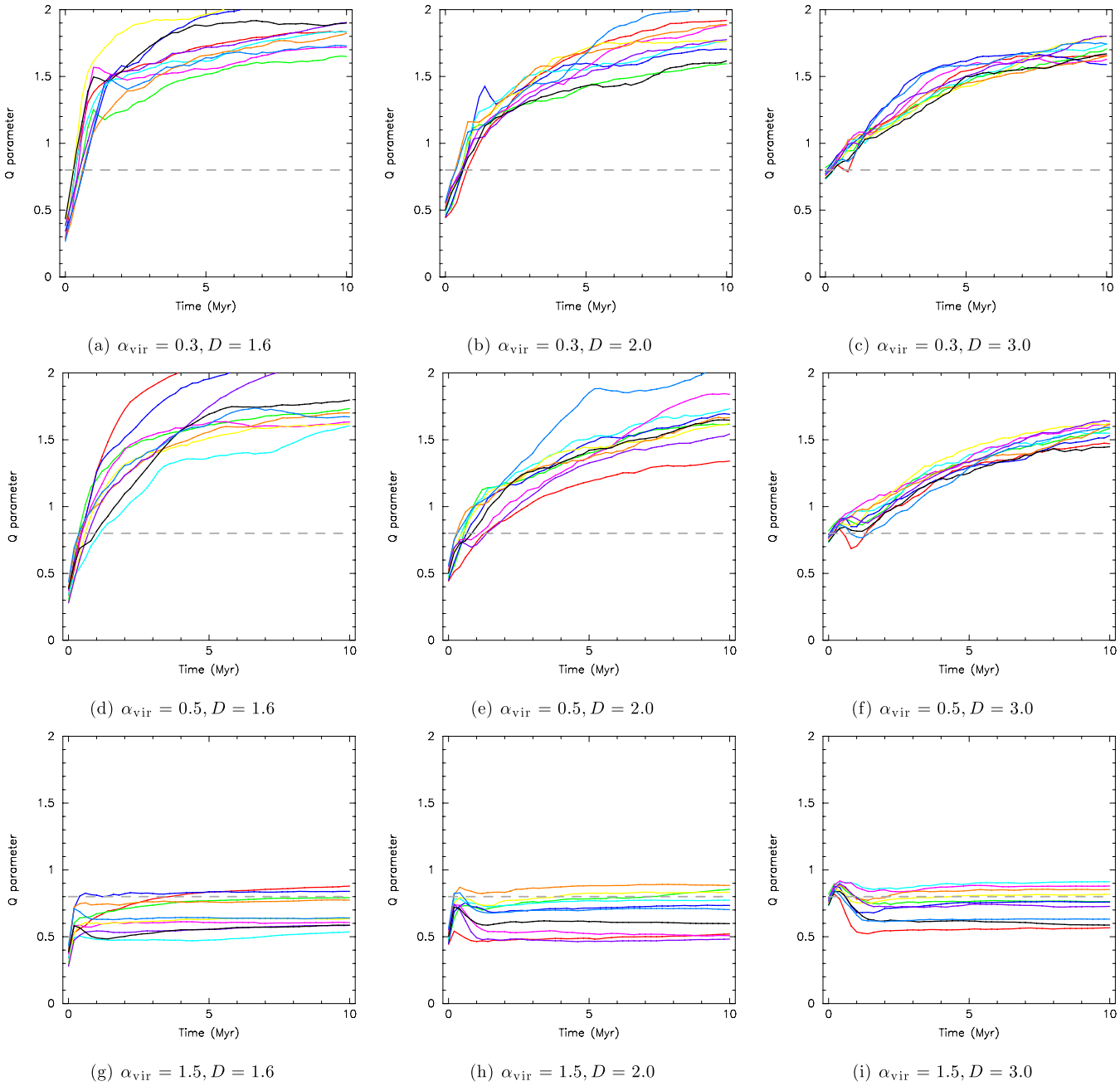

(a) $\alpha_{\rm vir} = 0.3, D = 1.6$ (b) $\alpha_{\rm vir} = 0.3, D = 2.0$ (c) $\alpha_{\rm vir} = 0.3, D = 3.0$

(d) $\alpha_{\rm vir} = 0.5, D = 1.6$ (e) $\alpha_{\rm vir} = 0.5, D = 2.0$ (f) $\alpha_{\rm vir} = 0.5, D = 3.0$

(g) $\alpha_{\rm vir} = 1.5, D = 1.6$ (h) $\alpha_{\rm vir} = 1.5, D = 2.0$ (i) $\alpha_{\rm vir} = 1.5, D = 3.0$

Figure 3. Evolution of the $\mathcal{Q}$-parameter with time for the simulations with $N = 1500$ stars. For clarity, we only show the first 10 simulations in each suite (we consider the $\mathcal{Q}$-parameter from all 20 simulations at several specific times in Figs 6 and 7).

collapse (more violently the lower both D and $\alpha_{\rm vir}$ are). This leads to an increase in $\Lambda_{\rm MSR}$ over the first few Myr as the massive stars come closer together and are able to dynamically mass segregate (see all panels a–f). But once dynamical mass segregation has occurred they can evolve in many ways. Especially in low-D and/or low-$\alpha_{\rm vir}$ regions hierarchical systems of massive stars can form which may violently decay (resulting in a rapid decline in $\Lambda_{\rm MSR}$ as seen above in Fig. 1 for our 'typical' cool system), or survive (resulting in $\Lambda_{\rm MSR}$ remaining high). Massive binaries can form that completely disrupt some regions. In some cases, the decay of the massive multiple system ejects high-mass stars resulting in a $\Lambda_{\rm MSR} < 1$ (inverse mass segregation).

4.3.3 *Evolution of* $\Sigma_{\rm LDR}$

In Fig. 5, we show the evolution of the $\Sigma_{\rm LDR}$ ratio for all nine sets of initial conditions (again, $N = 1500$ stars and $\alpha_{\rm vir} = 0.3, 0.5, 1.5$ for all of $D = 1.6, 2.0, 3.0$). As in Fig. 4, we plot the median $\Sigma_{\rm LDR}$ value for 20 simulations by the black cross (all values are for the 10 most massive stars). We show the 25 and 75 percentiles with the black bars, and indicate the extrema by the grey bars. Again note that the 'error bars' capture the range covered at each time, and that the evolution of each particular simulation's $\Sigma_{\rm LDR}$ can be very complicated.

We show $\Sigma_{\rm LDR} = 1$ by the solid red horizontal line. Usually, if $\Sigma_{\rm LDR} > 2$ the most massive stars have (statistically) significantly

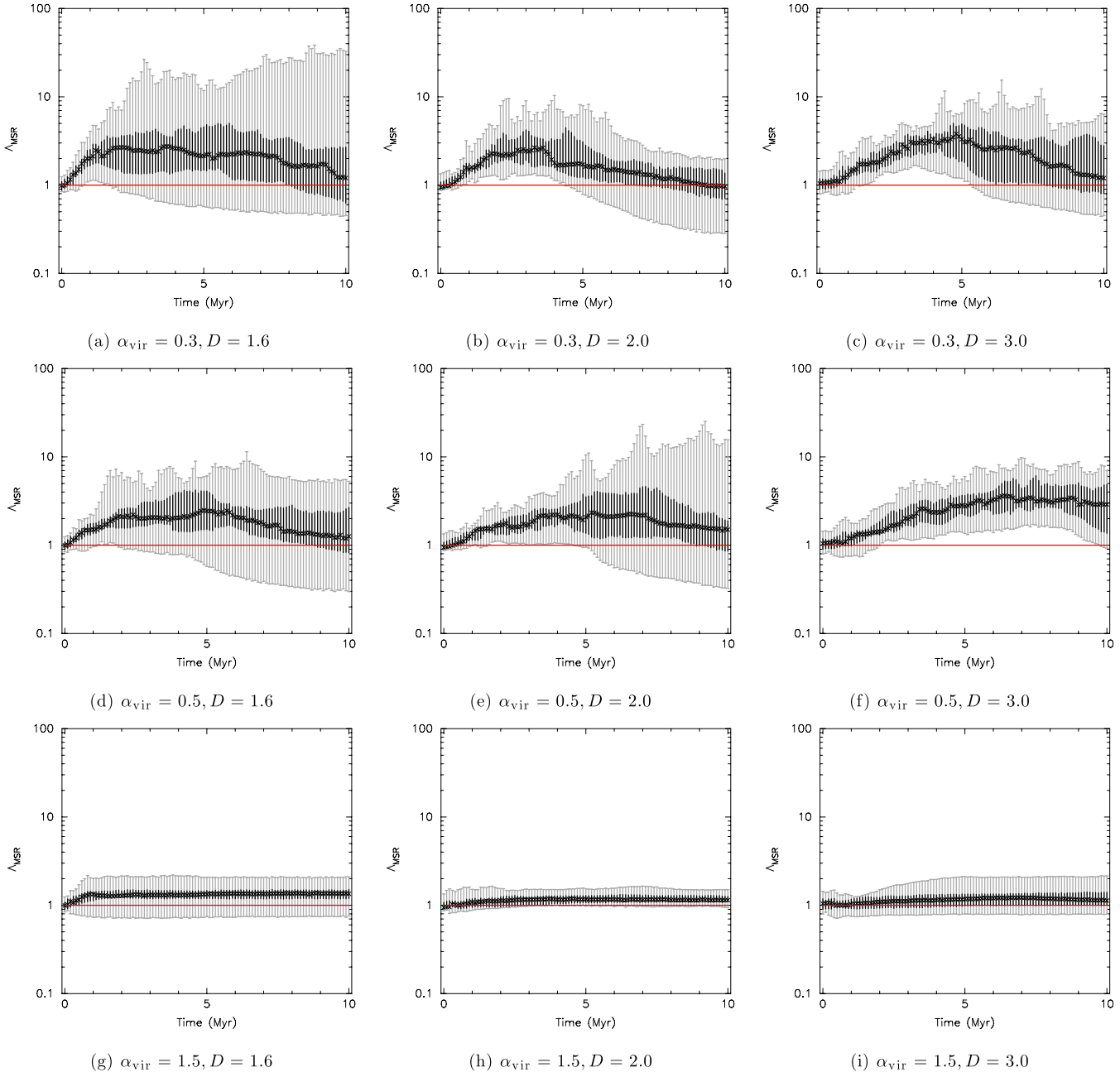

(a) $\alpha_{\rm vir} = 0.3, D = 1.6$ (b) $\alpha_{\rm vir} = 0.3, D = 2.0$ (c) $\alpha_{\rm vir} = 0.3, D = 3.0$

(d) $\alpha_{\rm vir} = 0.5, D = 1.6$ (e) $\alpha_{\rm vir} = 0.5, D = 2.0$ (f) $\alpha_{\rm vir} = 0.5, D = 3.0$

(g) $\alpha_{\rm vir} = 1.5, D = 1.6$ (h) $\alpha_{\rm vir} = 1.5, D = 2.0$ (i) $\alpha_{\rm vir} = 1.5, D = 3.0$

Figure 4. Evolution of $\Lambda_{\rm MSR}$ with time for simulations with $N = 1500$. Each panel shows the median $\Lambda_{\rm MSR}$ value of 20 simulations with identical initial conditions (the crosses) and the darker error bars indicate 25 and 75 percentile values. The entire range of possible values from the 20 sets of initial conditions is shown by the lighter error bars.

higher densities than the average stars in the region. Indeed, if we recall Figs 1(k) and 2(k), we see that the red circles (indicating an insignificant $\Sigma_{\rm LDR}$ ratio) are only present for $\Sigma_{\rm LDR} < 2$.

In contrast to $\Lambda_{\rm MSR}$, in *all* ensembles $\Sigma_{\rm LDR}$ tends to increase with time. Indeed, the median $\Sigma_{\rm LDR}$ by 10 Myr for almost all sets of initial conditions is very similar, with values of $\Sigma_{\rm LDR} \sim 5{-}10$. This means that the most massive stars almost always find themselves at significantly higher local surface densities than an average star, even in a hot, expanding region.

The time taken for $\Sigma_{\rm LDR}$ to increase depends on the level of substructure. In the first column with $D = 1.6$ (panels a, d and g) $\Sigma_{\rm LDR}$ rises to significant levels almost immediately. But in the third column with $D = 3.0$ (panels c, f and i) $\Sigma_{\rm LDR}$ takes a few Myr to reach significant levels.

The reason for this is that the massive stars act as a local potential well which can trap low-mass stars. $\Sigma_{\rm LDR}$ measures the size of the retinue of low (or high) mass stars collected by a massive star. If initial substructure is present, the high-mass star is likely to find itself with a ready-made retinue to attract, hence $\Sigma_{\rm LDR}$ rises very quickly. But when the stellar distribution is smooth it takes some time for the massive stars to collect a significant retinue of low-mass stars and so $\Sigma_{\rm LDR}$ rises more slowly. Indeed, the most significant

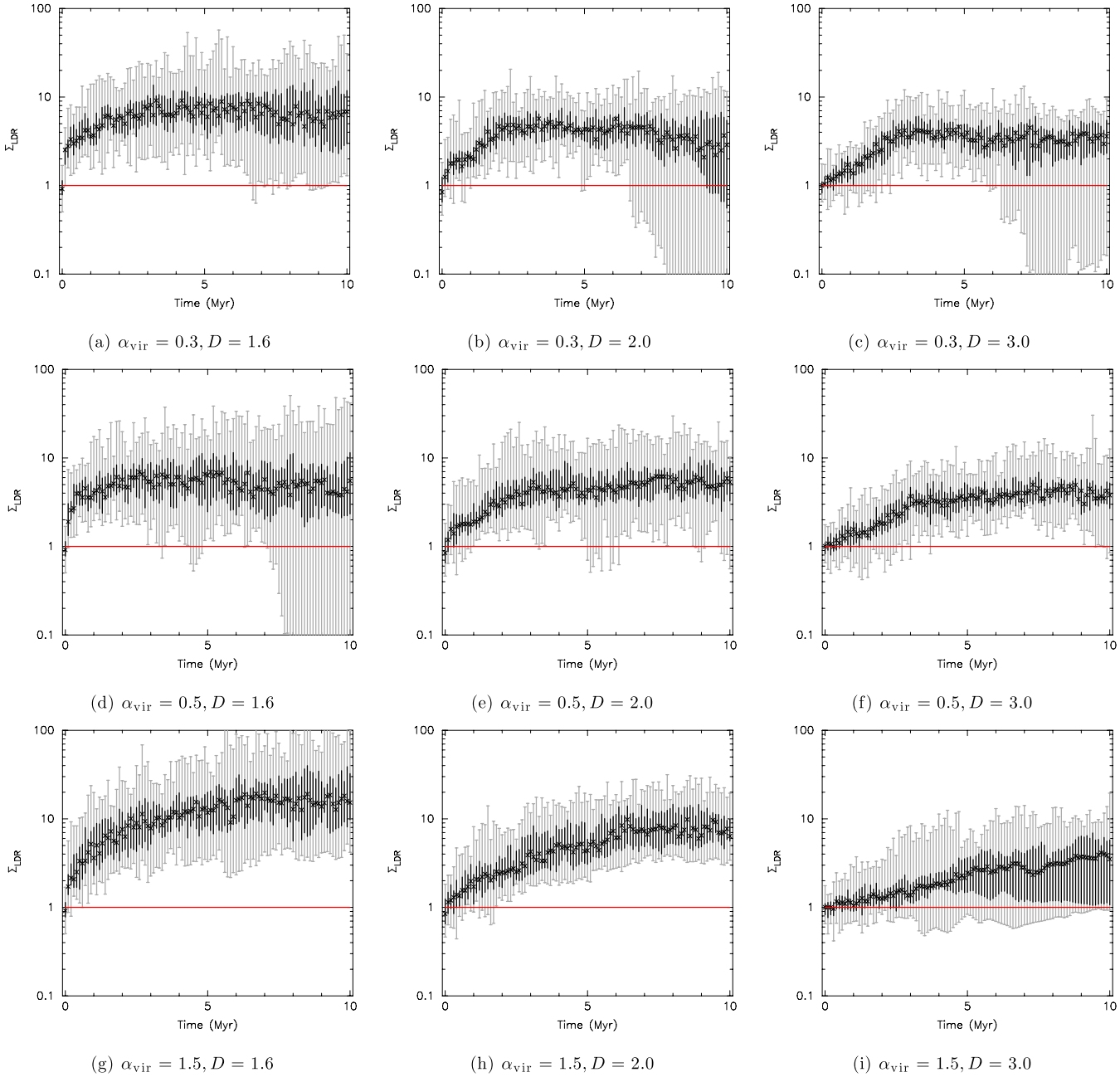

(a) $\alpha_{\rm vir} = 0.3, D = 1.6$ (b) $\alpha_{\rm vir} = 0.3, D = 2.0$ (c) $\alpha_{\rm vir} = 0.3, D = 3.0$

(d) $\alpha_{\rm vir} = 0.5, D = 1.6$ (e) $\alpha_{\rm vir} = 0.5, D = 2.0$ (f) $\alpha_{\rm vir} = 0.5, D = 3.0$

(g) $\alpha_{\rm vir} = 1.5, D = 1.6$ (h) $\alpha_{\rm vir} = 1.5, D = 2.0$ (i) $\alpha_{\rm vir} = 1.5, D = 3.0$

Figure 5. Evolution of $\Sigma_{\rm LDR}$ with time for simulations with $N = 1500$ stars. Each panel shows the median $\Sigma_{\rm LDR}$ value from 20 simulations with identical initial conditions (the crosses) and the darker error bars indicate 25 and 75 percentile values. The entire range of possible values from the 20 sets of initial conditions is shown by the lighter error bars.

rise in $\Sigma_{\rm LDR}$ is seen in the hottest and most substructured regions (panel g) where local substructure is bound and collected by the massive stars within a globally unbound region.

In a few cases, as seen in the large spread in extremes of $\Sigma_{\rm LDR}$ in panels (b) and (d) especially, the decay of higher order massive star multiples can eject massive stars without a retinue causing $\Sigma_{\rm LDR}$ to fall below unity (i.e. the massive stars have very low local densities). Allison & Goodwin (2011) showed that higher order Trapezium-like massive star systems are more likely to form at moderate D or $\alpha_{\rm vir}$ which is why panel (a) with the most extreme D and $\alpha_{\rm vir}$ does not show this decay and consequent $\Sigma_{\rm LDR} < 1$ values as it is much less likely to contain a relatively long-lived Trapezium-like system.

4.3.4 Structure versus mass segregation and local density

As shown in Fig. 3, the $\mathcal{Q}$-parameter measured at a given time can indicate the likely initial conditions of a star-forming region; something that is centrally concentrated after only 1–2 Myr is likely to have formed stars with either subvirial, or virial velocities. However, the large spread in possible values of $\mathcal{Q}$ means that any further inference of the initial conditions is not possible using $\mathcal{Q}$ alone. However, as pointed out by Allison et al. (2010) and demonstrated in Figs 4 and 5, the more subvirial and substructured a star-forming region is, the more likely mass segregation is to occur within 1 Myr (with the caveat that any residual gas potential does not strongly

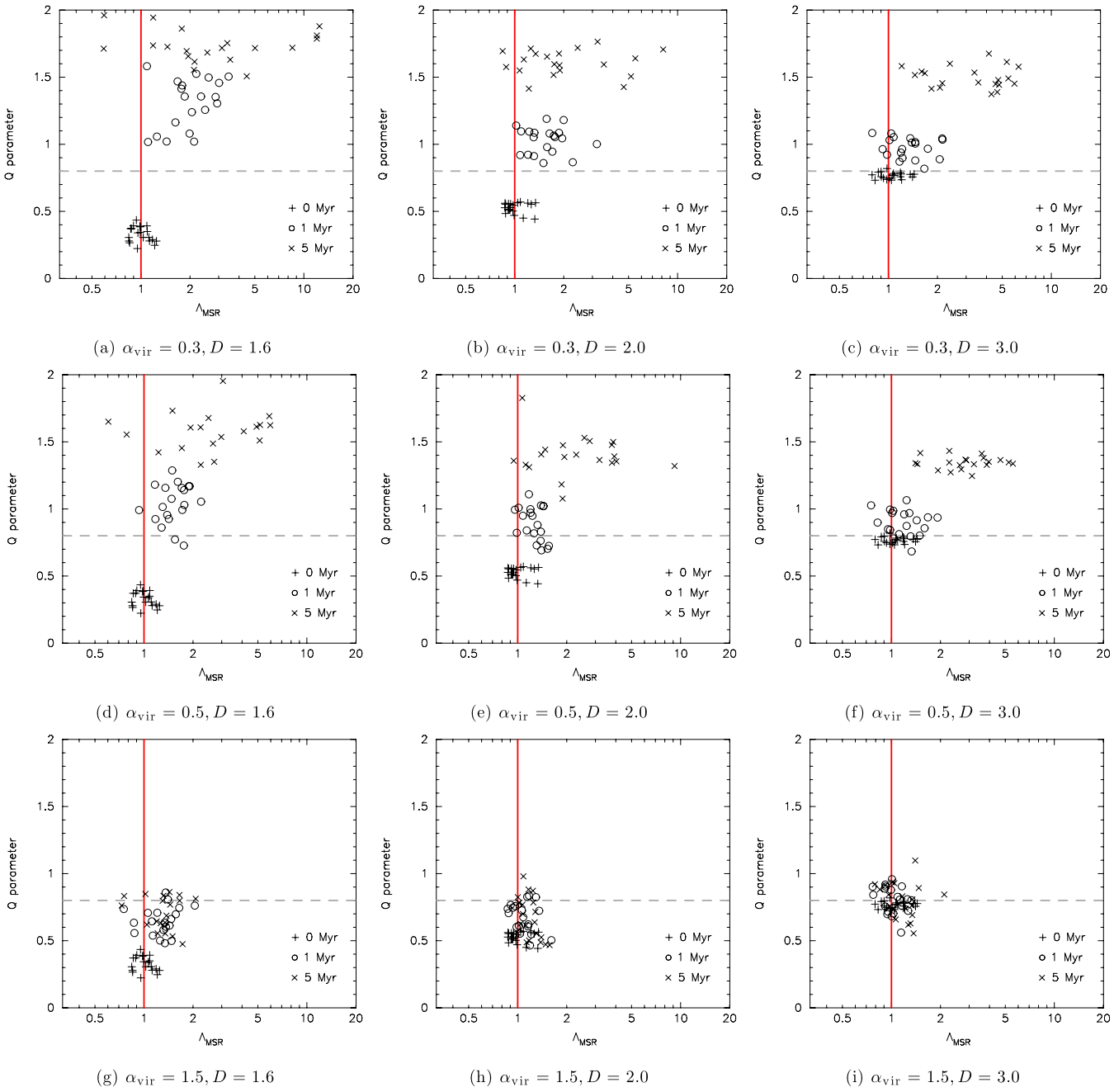

(a) $\alpha_{\rm vir} = 0.3, D = 1.6$ (b) $\alpha_{\rm vir} = 0.3, D = 2.0$ (c) $\alpha_{\rm vir} = 0.3, D = 3.0$

(d) $\alpha_{\rm vir} = 0.5, D = 1.6$ (e) $\alpha_{\rm vir} = 0.5, D = 2.0$ (f) $\alpha_{\rm vir} = 0.5, D = 3.0$

(g) $\alpha_{\rm vir} = 1.5, D = 1.6$ (h) $\alpha_{\rm vir} = 1.5, D = 2.0$ (i) $\alpha_{\rm vir} = 1.5, D = 3.0$

Figure 6. The evolution of $\mathcal{Q}$-parameter versus $\Lambda_{\rm MSR}$ with time for the simulations with $N = 1500$ stars. For each simulation, we plot the $\mathcal{Q}$-parameter and $\Lambda_{\rm MSR}$ at 0 Myr (the plus signs), 1 Myr (the open circles) and 5 Myr (the crosses). The boundary between substructured associations and radially smooth clusters ($\mathcal{Q} = 0.8$) is indicated by the horizontal grey dashed line, and $\Lambda_{\rm MSR} = 1$ is shown by the vertical red line.

affect the dynamical interactions – see Section 5). Furthermore, the level of mass segregation (if it occurs) is also higher for subvirial and substructured regions.

In Fig. 6, we plot the $\mathcal{Q}$-parameter against mass segregation ratio, $\Lambda_{\rm MSR}$, for each suite of $N = 1500$ stars simulations. We show the values at 0 Myr (i.e. before any dynamical evolution has taken place) by the plus signs, at 1 Myr (the open circles) and at 5 Myr (the crosses). The boundary between substructured and centrally concentrated morphologies ($\mathcal{Q} = 0.8$) is shown by the dashed grey line, and a mass segregation ratio of unity (i.e. no mass segregation) is shown by the solid red line.

For certain initial conditions ($\alpha_{\rm vir} = 0.3$, 0.5 – panels a–f), the evolution of the regions can be clearly seen in $\mathcal{Q} - \Lambda_{\rm MSR}$. However, it remains difficult to distinguish between subvirial and virial initial conditions. Furthermore, for the clusters with supervirial initial conditions (panels g–i) the plot is degenerate, as these regions do not mass segregate according to the definition of $\Lambda_{\rm MSR}$ (because the massive stars are unable to group together) and so the $\mathcal{Q} - \Lambda_{\rm MSR}$ values at different ages are overlaid.

In order to overcome the degeneracy in $\mathcal{Q} - \Lambda_{\rm MSR}$ space for regions with supervirial velocities, we also plot the $\mathcal{Q}$-parameter against the ratio of surface densities $\Sigma_{\rm LDR}$ for the simulations with

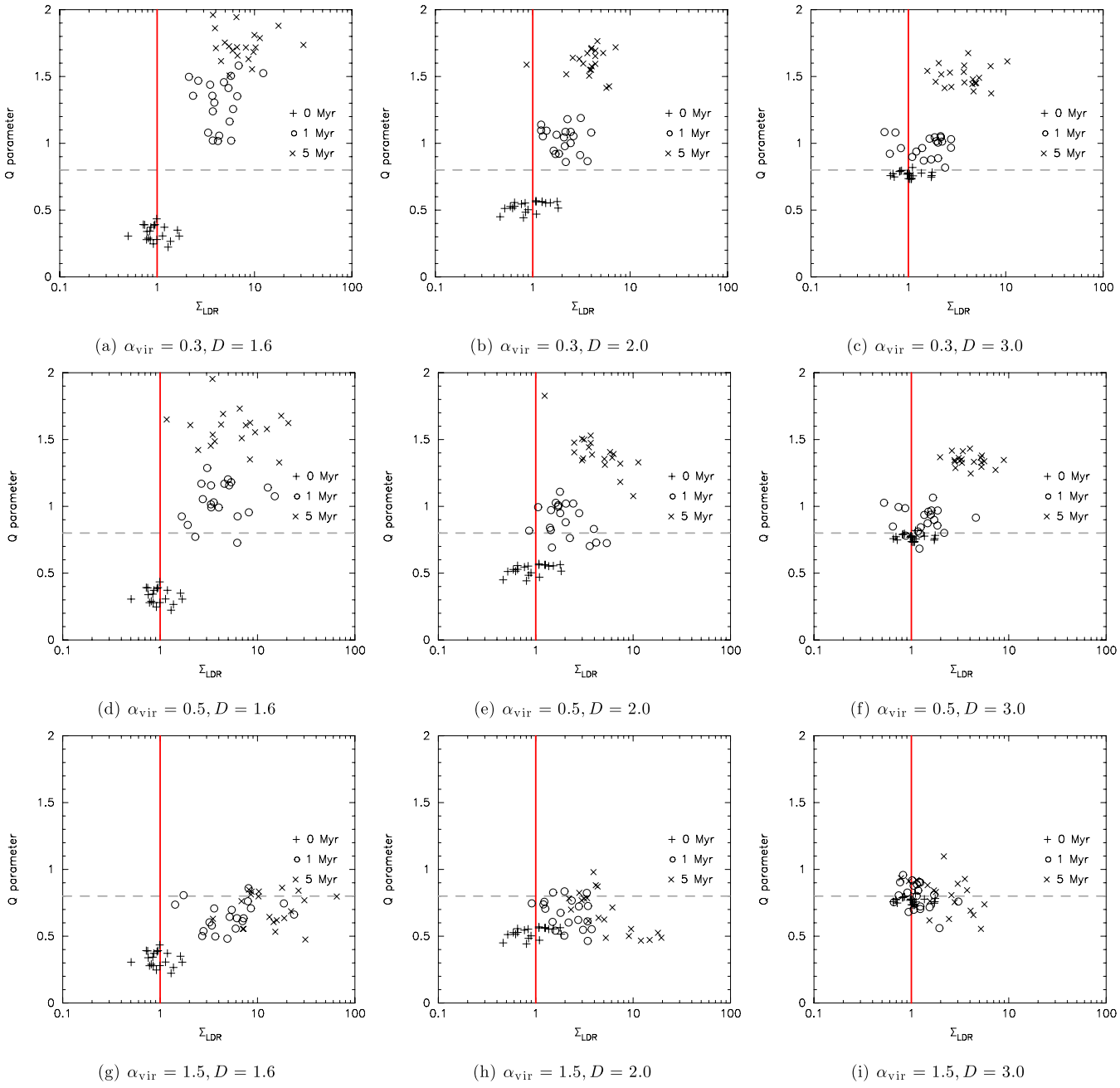

(a) $\alpha_{\rm vir} = 0.3, D = 1.6$ (b) $\alpha_{\rm vir} = 0.3, D = 2.0$ (c) $\alpha_{\rm vir} = 0.3, D = 3.0$

(d) $\alpha_{\rm vir} = 0.5, D = 1.6$ (e) $\alpha_{\rm vir} = 0.5, D = 2.0$ (f) $\alpha_{\rm vir} = 0.5, D = 3.0$

(g) $\alpha_{\rm vir} = 1.5, D = 1.6$ (h) $\alpha_{\rm vir} = 1.5, D = 2.0$ (i) $\alpha_{\rm vir} = 1.5, D = 3.0$

Figure 7. The evolution of $\mathcal{Q}$-parameter versus $\Sigma_{\rm LDR}$ with time for the simulations with $N = 1500$ stars. For each simulation, we plot the $\mathcal{Q}$-parameter and $\Sigma_{\rm LDR}$ at 0 Myr (the plus signs), 1 Myr (the open circles) and 5 Myr (the crosses). The boundary between substructured associations and radially smooth clusters ($\mathcal{Q} = 0.8$) is indicated by the horizontal grey dashed line, and $\Sigma_{\rm LDR} = 1$ is shown by the vertical red line.

$N = 1500$ stars in Fig. 7. In Fig. 7, we show the values at 0 Myr (i.e. before any dynamical evolution has taken place) by the plus signs, at 1 Myr (the open circles) and at 5 Myr (the crosses). The boundary between substructured and centrally concentrated morphologies ($\mathcal{Q} = 0.8$) is shown by the dashed grey line, and $\Sigma_{\rm LDR} = 1$ is shown by the solid red line. The $\mathcal{Q} - \Sigma_{\rm LDR}$ plot shows distinct differences between unevolved regions (the plus signs) and clusters with ages of 5 Myr (the crosses) for most initial conditions, and only becomes degenerate when the initial conditions are supervirial and not substructured (Fig. 7i).

Finally, we note that the initial densities of our simulations with $N = 1500$ stars may be higher than those observed in ∼50 per cent of nearby star-forming regions (Bressert et al. 2010; Parker & Meyer 2012). We therefore show the $\mathcal{Q} - \Sigma_{\rm LDR}$ plot for the low-density regions (initial median surface densities ∼100 stars pc^{-2}) in Fig. 8.

The dynamical evolution of these $N = 150$ regions is not as dramatic as in the higher N simulations. The reason for this is three-fold. First, lower-N results in lower number statistics and so the quantitative measures we are calculating are less significant. Secondly, lower N results in fewer stars to form retinues around the higher mass stars (and those higher mass stars are less likely to be significantly more massive than the average due to random sampling from the IMF). Finally, the lower N clusters have

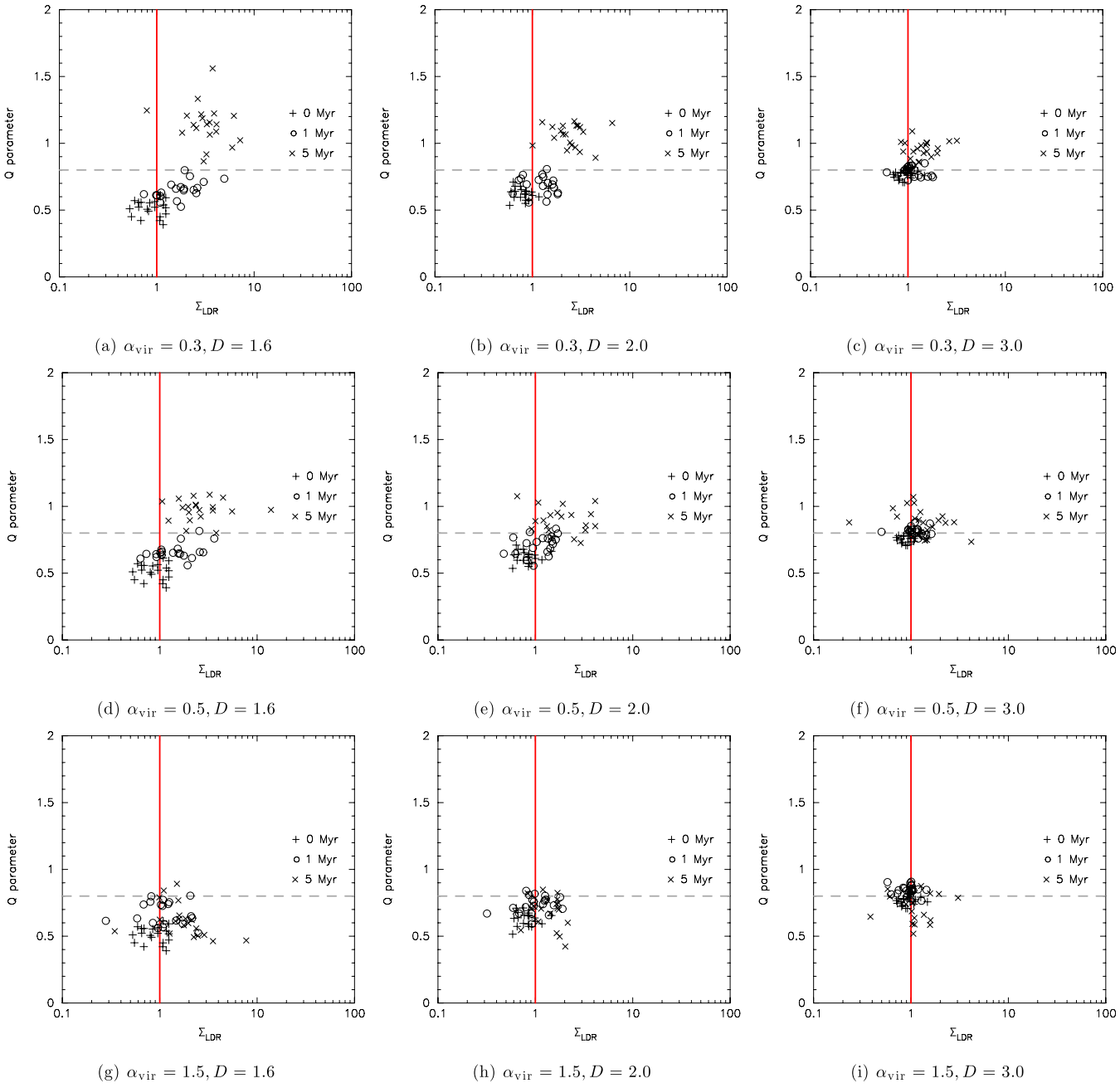

(a) $\alpha_{vir} = 0.3, D = 1.6$ (b) $\alpha_{vir} = 0.3, D = 2.0$ (c) $\alpha_{vir} = 0.3, D = 3.0$

(d) $\alpha_{vir} = 0.5, D = 1.6$ (e) $\alpha_{vir} = 0.5, D = 2.0$ (f) $\alpha_{vir} = 0.5, D = 3.0$

(g) $\alpha_{vir} = 1.5, D = 1.6$ (h) $\alpha_{vir} = 1.5, D = 2.0$ (i) $\alpha_{vir} = 1.5, D = 3.0$

Figure 8. The evolution of $\mathcal{Q}$-parameter versus Σ_{LDR} with time for the low-density ($N = 150$ stars) simulations. For each simulation, we plot the $\mathcal{Q}$-parameter and Σ_{LDR} at 0 Myr (the plus signs), 1 Myr (the open circles) and 5 Myr (the crosses). The boundary between substructured associations and radially smooth clusters ($\mathcal{Q} = 0.8$) is indicated by the horizontal grey dashed line, and $\Sigma_{LDR} = 1$ is shown by the vertical red line.

longer dynamical time-scales (for the same radius systems) than the larger N clusters, so that for the same physical age they will be dynamically less evolved (note that two-body relaxation is generally unimportant except in dynamically mass segregating regions that become dense, so the N-dependence of two-body relaxation is unimportant).

For these reasons, we can only readily distinguish between different epochs (0 and 5 Myr) in the $\mathcal{Q} - \Sigma_{LDR}$ plot when the simulations are substructured and subvirial ($\alpha_{vir} = 0.3$; $D = 1.6$, 2.0 – panels a and b in Fig. 8); i.e. when the evolution has been dramatic.

5 DISCUSSION

In the simulations presented in Section 4, we have seen that there are some trends (and some lack of trends) in the evolution of the quantitative structure parameters $\mathcal{Q}$, Λ_{MSR} and Σ_{LDR} with time. How these parameters evolve depends on the initial substructure present in a region (modelled by the fractal dimension, D, of the initial conditions), and the global dynamical 'temperature' of the region (modelled by the global virial ratio, α_{vir}).

It is very interesting to uncover the dynamics at work in the systems we have simulated. In common with past work, we have

found that substructure is erased in cool and tepid regions, but retained in hot regions (e.g. Goodwin & Whitworth 2004; Parker & Meyer 2012). Also following past work, we have found that the massive stars rapidly dynamically segregate in cool and tepid regions, but that the clusters so formed can evolve in different ways, and even destroy themselves (e.g. Allison et al. 2009b, 2010; Allison & Goodwin 2011).

The parameter space covered by Allison et al. did not include regions that initially expand (i.e. supervirial velocities). When regions have supervirial velocities, the massive stars usually have a similar spatial concentration to the average stars, and so the $\Lambda_{\rm MSR}$ technique does not find these associations to be mass segregated.

When using the $\Sigma - m$ method with its corresponding $\Sigma_{\rm LDR}$ local ratio, in nearly *all* regions the massive stars find themselves in regions of higher density than the median value in the cluster, irrespective of the initial amount of substructure, or virial ratio. Indeed, even in the regions which start as uniform spheres (Figs 5c, f and i) the 10 most massive stars have significantly higher surface densities than the average.

We attribute this to gravitational focusing from the massive stars, which act as potential wells and effectively 'sweep up' a retinue of low-mass stars as the region evolves [note the concentration of low-mass stars (shown by the black points) around the high-mass stars (the red triangles) in Figs 2b and c]. This means that the local surface density around high-mass stars almost always increases with time.

The evolution of spatial structure, as measured by the $\mathcal{Q}$-parameter, follows a similar pattern to the measures of mass segregation and local density. As noted by Parker & Meyer (2012), subvirial, substructured regions lose their structure much faster, and become more centrally concentrated, than virialized regions with smooth initial conditions (compare the $D = 1.6$, $\alpha_{\rm vir} = 0.3$ region in Fig. 3(a) with the $D = 3.0$, $\alpha_{\rm vir} = 0.5$ region in Fig. 3 f). Supervirial regions tend to erase some substructure, but remain substructured for the duration of the simulation as the stars in these models never fully mix together. However, a low $\mathcal{Q}$-parameter does not necessarily imply that the region is dynamically young, or that it has always been substructured to some degree. In Fig. 3(i), we see that several models that began as uniform spheres have developed substructure during their evolution.

Whilst an old (10 Myr) region with substructure may imply that the initial conditions were supervirial, or that the region is dynamically young, it is more informative to combine the $\mathcal{Q}$-parameter with the measures of mass segregation and local density to decide whether a star-forming region has undergone dynamical evolution. In Figs 6 and 7, we show the evolution of $\mathcal{Q}$ against $\Lambda_{\rm MSR}$, and $\mathcal{Q}$ against $\Sigma_{\rm LDR}$, respectively. The $\mathcal{Q} - \Lambda_{\rm MSR}$ plot (Fig. 6) shows that, for cool and tepid regions, structure is erased as the level of mass segregation increases. However, as dynamical evolution leads to massive stars attaining higher local densities than low-mass stars, the $\mathcal{Q} - \Sigma_{\rm LDR}$ plot (Fig. 7) enables us to determine whether dynamical evolution has taken place, and if so, to distinguish between initially cool/tepid and hot regions (i.e. bound clusters versus unbound associations).

The most obvious question to ask is to what extent these results can be applied to real observations of a single snapshot in the evolution of a real star-forming region?

Before we do this, it is worth quickly discussing the difference between physical and dynamical ages. Two systems with the same physical age (say, 1 Myr), can have very different dynamical ages. The dynamical age is a measure of how much the system can have relaxed into a rough equilibrium. To first order, the dynamical age is the number of crossing times old the system is. Gieles & Portegies Zwart (2011) define a 'cluster' as distinct from an 'association' from the number of crossing times old a system is. An unbound system is, by definition, always less than a crossing time old (they define this as an association). A bound system can be more than one crossing time old (a cluster). However, in the very young systems we are considering, even if a system is bound it may still be dynamically young in that it is only one or two crossing times old.

The evolution of $\mathcal{Q}$ we find above is a proxy of dynamical age. Relaxation will increase $\mathcal{Q}$ as substructure is erased, therefore with increasing dynamical age we have increasing $\mathcal{Q}$.

5.1 Comparison with observations

What might we say from real observations of $\mathcal{Q}$, $\Lambda_{\rm MSR}$ and $\Sigma_{\rm LDR}$? The key parameter is $\mathcal{Q}$, which provides an upper limit on the initial $\mathcal{Q}$, and hence the initial degree of substructure in the region. Here, we discuss three different regimes of $\mathcal{Q}$.

Low $\mathcal{Q}$ ($\mathcal{Q} < 0.8$ or 1). If a region has a low $\mathcal{Q}$ then *it must be dynamically young*. It has not managed to erase its substructure, and is not well mixed.

In dynamically young regions $\Lambda_{\rm MSR}$ provides a measure of how well separated the massive stars were at birth. In our simulations, we randomly place the massive stars and so for low $\mathcal{Q}$ we always find $\Lambda_{\rm MSR} \sim 1$. If we observed a low $\mathcal{Q}$ but a $\Lambda_{\rm MSR}$ value significantly above or below unity this would provide information on the formation of massive stars relative to low-mass stars.

Even if a region is globally dynamically young, locally (especially around massive stars) it might be dynamically older. We find that $\Sigma_{\rm LDR}$ increases with time as the massive stars gain a retinue of low-mass stars. Therefore, the observed value of $\Sigma_{\rm LDR}$ is an upper limit on the initial $\Sigma_{\rm LDR}$.

High values of $\Sigma_{\rm LDR}$ with low $\mathcal{Q}$ are probably indicative of a high degree of initial substructure acting as seeds for massive stars to gain a retinue (see panels g–i of Fig. 7).

Moderate $\mathcal{Q}$ ($\mathcal{Q} \sim 1$). Regions with moderate $\mathcal{Q}$ may have formed with moderate $\mathcal{Q}$ and be dynamically young (i.e. not have changed their structure much since birth). Alternatively, they may have formed with low $\mathcal{Q}$ and have undergone a small degree of violent relaxation. They cannot be globally dynamically old.

In our simulations with no initial mass segregation we find that when $\mathcal{Q} \sim 1$ that $\Lambda_{\rm MSR}$ is around 1–2 (i.e. hardly significant). An observation of a significant $\Lambda_{\rm MSR}$ in a moderate $\mathcal{Q}$ region would strongly suggest that the massive stars formed with a significant $\Lambda_{\rm MSR}$ (i.e. they were initially mass segregated).

However, we do find a wide range in $\Sigma_{\rm LDR}$ for moderate $\mathcal{Q}$ (see again panels g–i of Fig. 7). Again, high values of $\Sigma_{\rm MSR}$ with moderate $\mathcal{Q}$ are probably indicative of a high degree of initial substructure.

High $\mathcal{Q}$ ($\mathcal{Q} > 1.5$). Regions with high $\mathcal{Q}$ could be dynamically very old and have erased their substructure (i.e. the 5 Myr old systems in panels a–f of Figs 6 and 7). Or they may have formed with a high $\mathcal{Q}$. After only 1 Myr cool regions have erased their substructure and are indistinguishable (by $\mathcal{Q}$) from regions that formed centrally concentrated.

With no initial mass segregation high $\mathcal{Q}$ regions rapidly increase both $\Lambda_{\rm MSR}$ and $\Sigma_{\rm LDR}$ meaning they are indistinguishable from systems that started with high $\Lambda_{\rm MSR}$ and $\Sigma_{\rm LDR}$. And by 5 Myr the evolution is such that almost any value of $\Lambda_{\rm MSR}$ and $\Sigma_{\rm LDR}$ is

associated with high $\mathcal{Q}$ regions. Typically, $\Sigma_{\rm LDR}$ is high at late times in high $\mathcal{Q}$, but there are outliers in which it is not.

5.1.1 *ρ Oph, Taurus and Cyg OB2*

There are three young regions for which we have information in the literature on $\mathcal{Q}$, $\Lambda_{\rm MSR}$ and $\Sigma_{\rm LDR}$.

Parker et al. (2012) analyse ρ Oph and find for this ∼1 Myr region that $\Lambda_{\rm MSR} \sim 1$, and $\Sigma_{\rm LDR} \sim 1$ (no evidence for any mass segregation or massive stars residing in overdensities). From Cartwright & Whitworth (2004) we have $\mathcal{Q} = 0.85$ for ρ Oph.

Examination of Fig. 7 shows that several sets of initial conditions have $\Sigma_{\rm LDR} \sim 1$ and $\mathcal{Q} = 0.85$ at 1 Myr. These tend to have tepid or hot initial conditions, and relatively high fractal dimensions.

The best bet for ρ Oph is that it formed with a $\mathcal{Q}$ similar to what we see now, and is dynamically young. It could be globally bound or unbound, and without dynamical information it is impossible to tell. But we are probably seeing something with a global structure not too dissimilar to that with which it formed.

However, it should be noted that ρ Oph only contains ∼250 members (e.g. Alves de Oliveira et al. 2012) meaning that any quantitative measure, and especially $\Lambda_{\rm MSR}$, and $\Sigma_{\rm LDR}$ will be rather noisy (see Section 4.3.4).

For Taurus, Cartwright & Whitworth (2004) find $\mathcal{Q} = 0.47$ (extremely substructured). Parker et al. (2011) find that $\Lambda_{\rm MSR} \sim 0.7$ (it is inversely mass segregated). Kirk & Myers (2011) perform an analysis of subgroups of Taurus which is not too dissimilar to $\Sigma_{\rm LDR}$ and find *local* mass segregation.

The very low global value of $\mathcal{Q}$ shows that globally Taurus is dynamically young (an unsurprising result given the roughly 20 pc extent of this 1 Myr old region). As discussed by Parker et al. (2011), the $\Lambda_{\rm MSR} \sim 0.7$ is therefore probably primordial as dynamics have had no opportunity to change the global structure. However, the local mass segregation in groups could suggest that subclusters are dynamically old (given their sub-pc sizes this is very likely).

In a recent paper, Wright et al. (2014) find that the massive association Cyg OB2 has a low $\mathcal{Q}$-parameter ($\mathcal{Q} \sim 0.4 - 0.5$) and no evidence for mass segregation or massive stars residing in overdensities ($\Lambda_{\rm MSR} = 1.14$ and $\Sigma_{\rm LDR} = 1.44$), based on data collated in Wright et al. (2010). This strongly suggests that Cyg OB2 has not undergone any significant dynamical evolution, and probably formed with a similar morphology and density to that currently observed; i.e. a sparse ($\tilde{\Sigma} = 19$ stars pc^{-2}, Wright et al. 2014), unbound association.

5.2 Caveats and assumptions

Our main result is that the $\mathcal{Q} - \Sigma_{\rm LDR}$ plot (Fig. 7) enables us determine whether dynamical evolution has taken place, and if so, to distinguish between initially cool/tepid and hot regions (i.e. bound clusters versus unbound associations).

We find that the massive stars only acquire a retinue of low-mass stars if the initial density of the region is relatively high. Our model fractals have initial median local surface densities of ∼5000 stars pc^{-2} (the blue dashed lines in Figs 1g and 2g). If we plot the evolution of $\mathcal{Q} - \Sigma_{\rm LDR}$ for fractals with initial median surface densities of ∼100 stars pc^{-2}, then little dynamical evolution occurs and the $\mathcal{Q} - \Sigma_{\rm LDR}$ plot becomes degenerate in time (Fig. 8). This (surface) density threshold of 100 stars pc^{-2} corresponds to a volume density threshold of 100 stars pc^{-3} because the depth scale of the simulations is of the order of 1 pc.

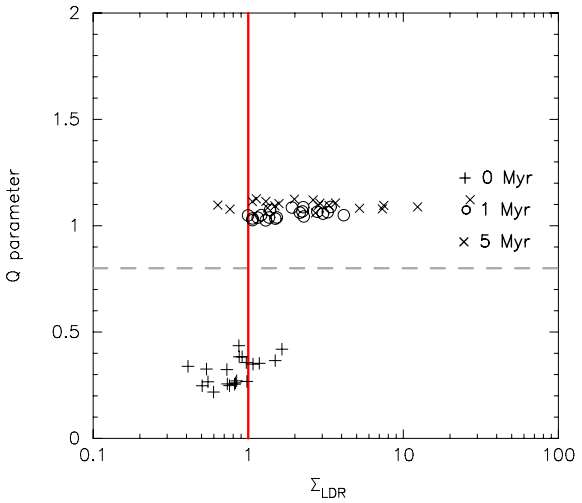

Figure 9. As Fig. 7(g), but for regions where the velocities of stars are not correlated. All substructure is erased, and fewer models show overdensities around massive stars according to the $\Sigma_{\rm LDR}$ method, than in the case of correlated velocities.

A recent analysis of simulations of high-mass star formation by Parker & Dale (2013) did not find any evidence for primordial mass segregation in regions which form in hydrodynamical simulations, nor did they find evidence for subsequent accumulation of retinues according to the $\Sigma - m$ method. In those simulations, the initial median surface density was similar to that of the low-density regions modelled here, and this result is consistent with the lack of high $\Sigma_{\rm LDR}$ ratios in Fig. 8. This returns us to the distinction between physical and dynamical ages. The relatively higher initial (surface) densities of our initial conditions reduce the dynamical (crossing) times of our simulations relative to lower densities – 5 Myr of physical time in Fig. 8 corresponds to less dynamical time than 5 Myr of physical time in Fig. 7.

Aside from the initial density, another assumption in our simulations is that the velocities of stars are correlated by distance. If we remove any correlation, and simply draw velocities from a Gaussian distribution and scale to the required virial ratio, we remove any initial substructure on very fast (<1 Myr) time-scales (Fig. 9). Therefore, in order to distinguish between bound clusters and unbound associations using the $\mathcal{Q} - \Sigma_{\rm LDR}$ plot, we require the (reasonable) assumption that the velocities of stars are initially correlated on local scales (Larson 1981).

The competitive accretion theory of star formation predicts that the most massive stars should be primordially mass segregated (e.g. Zinnecker 1982; Bonnell et al. 2003), and such behaviour is seen in *some* simulations of massive star formation (Maschberger & Clarke 2011), but not in others (Dale et al. 2012, 2013; Girichidis et al. 2012; Parker & Dale 2013). Whilst mass segregation is observed in some clusters (Hillenbrand & Hartmann 1998; Allison et al. 2009a; Sana et al. 2010; Pang et al. 2013), it may occur purely due to dynamical interactions (Allison et al. 2010) as it is not observed in some clusters and associations which are dynamically young (Parker et al. 2011, 2012; Delgado et al. 2013; Wright et al. 2014). Alternatively, the observed levels of mass segregation (when it is present) in clusters could be a combination of some primordial segregation, with later dynamical segregation (Moeckel & Bonnell 2009a).

In our simulations, we see that $\Sigma_{\rm LDR}$ always increases with time. We started with no mass segregation or high local densities around

massive stars, but even if we had started with $\Sigma_{\rm LDR} > 1$, then $\Sigma_{\rm LDR}$ should still tend to increase. But if we make the assumption of no *initial* mass segregation, then observed values of $\mathcal{Q}$ and $\Sigma_{\rm LDR}$ can be used to estimate the initial density of the region.

The dynamical evolution of substructured regions is highly stochastic. Two regions with (statistically) identical initial conditions can exhibit very different degrees of mass segregation, which can occur at different times in the regions' evolution. Similarly, Parker & Meyer (2012) find a large scatter in the evolution of $\mathcal{Q}$-parameter and median surface density; and Parker & Goodwin (2012) find a large scatter in the evolution of binary star orbital properties, in substructured regions. Using the $\mathcal{Q}$-parameter in isolation is not enough to determine whether or not a star-forming region has undergone dynamical evolution, and should be coupled with the $\Sigma_{\rm LDR}$ ratio of mass-weighted local density. Recent work by Delgado et al. (2013) considered both the $\mathcal{Q}$-parameter and $\Lambda_{\rm MSR}$, but adopted the median MST length. This is in some ways analogous to using the $\Sigma_{\rm LDR}$ ratio, and these authors argued for different initial conditions for the clusters Berkeley 94 and Berkeley 96 (the former likely to have undergone warm expansion, and the latter cool collapse).

Our simulations are pure *N*-body models, and as such do not include the effects of gas left over from the star formation process. If star formation is inefficient, then previous studies have suggested that the rapid removal of this gas from a star-forming region will dominate its subsequent evolution (e.g. Tutukov 1978; Whitworth 1979; Lada, Margulis & Dearborn 1984; Goodwin 1997; Goodwin & Bastian 2006; Baumgardt & Kroupa 2007; Parmentier & Pfalzner 2013, and many others).

However, these (and other) studies usually assume that the stars and gas are well coupled; i.e. that the spatial distribution of the stars and gas is similar, and that the stars are in equilibrium with the gas. It is highly unclear if either of these assumptions is true.

Goodwin (2009) showed that the dynamical state of the stars is crucial to how they react to gas expulsion, slow-moving stars will 'feel' the effects of gas expulsion far less than fast-moving stars (relative to their equilibrium values). Recent work analysing hydrodynamical simulations of star formation has shown that when the stars and gas are decoupled (Offner, Hansen & Krumholz 2009), then the regions where stars form tend to be gas poor and so the influence of gas expulsion on the cluster's evolution is minimal (Kruijssen et al. 2012). In such a scenario, the subsequent dynamical evolution of the cluster is then dominated by two-body interactions, rather than gas removal (e.g. Smith et al. 2011; Gieles, Moeckel & Clarke 2012; Moeckel et al. 2012). This appears to be the case in some observed young massive clusters, which are gas free, but still (sub-)virial, implying that gas expulsion has had little, or no effect (Rochau et al. 2010; Cottaar et al. 2012). Smith et al. (2011) also showed that substructure in the stellar distribution during gas expulsion can be extremely important in the response of a system to gas expulsion (the albeit simple case of a smooth external gas potential).

This does not, of course, mean that we should completely neglect the effects of gas on the evolution of star-forming regions, even if they are modest. Recent advances in code development have enabled a better treatment of gas to be included in *N*-body simulations (e.g. Moeckel & Clarke 2011; Pelupessy & Portegies Zwart 2012; Fujii & Portegies Zwart 2013; Hubber et al. 2013), and such codes will be used in future studies.

Finally, we note that in our simulations we have access to the full, three-dimensional spatial data. However, even if we use only the 2D data and remove stars that lie outside two half-mass radii, the results do not change by much and we are still able to distinguish between bound and unbound star formation using the $\mathcal{Q} - \Sigma_{\rm LDR}$ plot.

5.3 Kinematics and the influence of binaries

In this paper, we have deliberately refrained from presenting information on the velocities of stars in the simulations, such as the velocity dispersion as a function of stellar mass. Our reasons for doing this are two-fold; first, although velocity dispersions are available for some clusters (e.g. Bosch et al. 2001; Gieles, Sana & Portegies Zwart 2010; Rochau et al. 2010; Cottaar et al. 2012; Hénault-Brunet et al. 2012) and associations (e.g. Steenbrugge et al. 2003; Kiminki et al. 2007), the data are often restricted to a narrow stellar mass range (e.g. Cottaar et al. 2012), making detailed comparisons with simulations difficult. Here it should be noted that ongoing spectroscopic surveys, such as the European Southern Observatory VLT/FLAMES programme (Randich 2012), and the Apache Point Observatory Galactic Evolution Experiment (APOGEE) survey (Zasowski et al. 2013) could soon remedy this issue. Secondly, the development of other quantitative measures of the dynamical state of a cluster using radial velocity measurements is currently in its infancy. Cartwright (2009) adapted the $\mathcal{Q}$-parameter for use with radial velocity measurements, but found that the use of the third spatial dimension instead of radial velocities gave better results. However, in future work we will analyse our simulations in greater detail to search for observational diagnostics in velocity space.

We note that the *Gaia* satellite (and associated spectroscopic surveys) have the potential to distinguish between field stars and cluster members on the periphery of embedded and young open clusters, which could facilitate a direct comparison with runaway stars in simulations (Allison 2012), and even trace back individual field stars to their natal regions (Moyano Loyola & Hurley 2013).

For simplicity, the simulations presented here do not contain any primordial binaries. Whilst the binary populations in star-forming regions are not as well constrained as in the Galactic field (King et al. 2012a,b; Duchêne & Kraus 2013), the semimajor axis distributions are, to zeroth order, similar to the field (King et al. 2012b) and the distributions of mass ratios also are consistent with the field (Metchev & Hillenbrand 2009; Reggiani & Meyer 2011, 2013).

The presence of primordial binaries is likely to influence the degree to which a system mass segregates, although this needs to be tested fully as all simulations have so far neglected binaries (e.g. Allison et al. 2010; Olczak, Spurzem & Henning 2011; Yu, de Grijs & Chen 2011). Due to their increased system mass, massive star binaries could in principle facilitate a higher degree of mass segregation because the mass segregation time-scale is a function of relative stellar mass (Spitzer 1969), although this may be balanced by an increased frequency of ejections of massive stars from unstable Trapezium-like systems (Allison & Goodwin 2011). Recently, Geller et al. (2013) showed that the binary fraction as a function of distance from the cluster centre could be an indicator of the amount of dynamical mass segregation that has taken place in the cluster. We plan to make a full assessment of the impact of primordial binaries on the $\mathcal{Q}$-parameter, $\Lambda_{\rm MSR}$ and $\Sigma_{\rm LDR}$ in future studies.

6 CONCLUSIONS

In this paper, we have modelled the dynamical evolution of star-forming regions with $N = 1500$ or $N = 150$ stars and varied the

amount of initial substructure and the initial bulk motion of the stars. We have searched for mass segregation, and increases in the local density around massive stars, and compared these to the evolution of the spatial structure of stars over a 10 Myr timeframe. Our conclusions are the following.

(i) The level of substructure in a region, as measured by the $\mathcal{Q}$-parameter generally stays the same or increases with (dynamical) age. Low values of $\mathcal{Q}$ show that a region is dynamically young (see also Parker & Meyer 2012).

(ii) The surface density around massive stars, as measured by the $\Sigma - m$ technique generally increases with time. This is due to massive stars collecting a retinue of low-mass stars.

(iii) The relative closeness of massive stars, as measured by the $\Lambda_{\rm MSR}$ method, stays the same or increases at first, but can evolve in many different ways according to the details of the dynamics in any situation (see also Allison et al. 2009).

We have introduced the $\mathcal{Q} - \Sigma_{\rm LDR}$ plot, which traces the dynamical evolution of a star forming and removes (some of) the degeneracies of using the $\mathcal{Q}$-parameter in isolation. Combining $\mathcal{Q}$ and $\Sigma_{\rm LDR}$ (and $\Lambda_{\rm MSR}$ can certainly help) can provide information on the initial energy (boundness), dynamical age, initial structure, initial density and initial degree of mass segregation of star-forming regions from the instantaneous projected positions and masses of the stars.

Finally, we note that the upcoming *Gaia* space telescope, and associated ground-based spectroscopic surveys, will soon add a wealth of information on stellar velocities in star-forming regions, clusters and associations. If used in tandem with the analysis of spatial distributions such as the $\mathcal{Q} - \Sigma_{\rm LDR}$ plot, we will be able to characterize the dynamical state (and hence initial conditions) of star-forming regions, clusters and associations.

ACKNOWLEDGEMENTS

We thank the anonymous referee for their comments and suggestions, which improved the original manuscript. NJW acknowledges a Royal Astronomical Society Research Fellowship. The simulations in this work were performed on the BRUTUS computing cluster at ETH Zürich. Part of this work was developed during an International Team programme at the International Space Science Institute, Bern, Switzerland.

REFERENCES

Allison R. J., 2012, MNRAS, 421, 3338
Allison R. J., Goodwin S. P., 2011, MNRAS, 415, 1967
Allison R. J., Goodwin S. P., Parker R. J., Portegies Zwart S. F., de Grijs R., Kouwenhoven M. B. N., 2009a, MNRAS, 395, 1449
Allison R. J., Goodwin S. P., Parker R. J., de Grijs R., Portegies Zwart S. F., Kouwenhoven M. B. N., 2009b, ApJ, 700, L99
Allison R. J., Goodwin S. P., Parker R. J., Portegies Zwart S. F., de Grijs R., 2010, MNRAS, 407, 1098
Alves de Oliveira C., Moraux E., Bouvier J., Bouy H., 2012, A&A, 539, A151
André P. et al., 2010, A&A, 518, L102
Bastian N., Gieles M., Ercolano B., Gutermuth R., 2009, MNRAS, 392, 868
Bastian N., Covey K. R., Meyer M. R., 2010, ARA&A, 48, 339
Bate M. R., 2012, MNRAS, 419, 3115
Baumgardt H., Kroupa P., 2007, MNRAS, 380, 1589
Bonnell I. A., Davies M. B., 1998, MNRAS, 295, 691
Bonnell I. A., Bate M. R., Clarke C. J., Pringle J. E., 2001, MNRAS, 323, 785
Bonnell I. A., Bate M. R., Vine S. G., 2003, MNRAS, 343, 413
Bonnell I. A., Clark P. C., Bate M. R., 2008, MNRAS, 389, 1556
Bosch G., Selman F., Melnick J., Terlevich R., 2001, A&A, 380, 137
Bressert E. et al., 2010, MNRAS, 409, L54
Carpenter J. M., Meyer M. R., Dougados C., Strom S. E., Hillenbrand L. A., 1997, AJ, 114, 198
Cartwright A., 2009, MNRAS, 400, 1427
Cartwright A., Whitworth A. P., 2004, MNRAS, 348, 589
Cartwright A., Whitworth A. P., 2009, MNRAS, 392, 341
Casertano S., Hut P., 1985, ApJ, 298, 80
Chabrier G., 2003, PASP, 115, 763
Chabrier G., 2005, in Corbelli E., Palle F., eds, Astrophysics and Space Science Library, Vol. 327, The Initial Mass Function: From Salpeter 1955 to 2005. Springer-Verlag, Berlin, p. 41
Cottaar M., Meyer M. R., Andersen M., Espinoza P., 2012, A&A, 539, A5
Dale J. E., Ercolano B., Bonnell I. A., 2012, MNRAS, 424, 377
Dale J. E., Ercolano B., Bonnell I. A., 2013, MNRAS, 430, 234
Delgado A. J., Djupvik A. A., Costado M. T., Alfaro E. J., 2013, MNRAS, 435, 429
Duchêne G., Kraus A., 2013, ARA&A, 51, 269
Elmegreen B. G., Elmegreen D. M., 2001, AJ, 121, 1507
Fujii M. S., Portegies Zwart S., 2013, preprint (arXiv:1309.1223)
Geller A. M., de Grijs R., Li C., Hurley J. R., 2013, ApJ, preprint (arXiv:1310.1085)
Gieles M., Portegies Zwart S. F., 2011, MNRAS, 410, L6
Gieles M., Sana H., Portegies Zwart S. F., 2010, MNRAS, 402, 1750
Gieles M., Moeckel N., Clarke C. J., 2012, MNRAS, 426, L11
Girichidis P., Federrath C., Allison R., Banerjee R., Klessen R. S., 2012, MNRAS, 420, 3264
Goodwin S. P., 1997, MNRAS, 286, 669
Goodwin S. P., 2009, Ap&SS, 324, 259
Goodwin S. P., Bastian N., 2006, MNRAS, 373, 752
Goodwin S. P., Whitworth A. P., 2004, A&A, 413, 929
Gouliermis D., Keller S. C., Kontizas M., Kontizas E., Bellas-Velidis I., 2004, A&A, 416, 137
Gouliermis D. A., de Grijs R., Xin Y., 2009, ApJ, 692, 1678
Hénault-Brunet V. et al., 2012, A&A, 546, A73
Hillenbrand L. A., Hartmann L. W., 1998, ApJ, 492, 540
Hubber D. A., Allison R. J., Smith R., Goodwin S. P., 2013, MNRAS, 430, 1599
Kiminki D. C. et al., 2007, ApJ, 664, 1102
King R. R., Parker R. J., Patience J., Goodwin S. P., 2012a, MNRAS, 421, 2025
King R. R., Goodwin S. P., Parker R. J., Patience J., 2012b, MNRAS, 427, 2636
Kirk H., Myers P. C., 2011, ApJ, 727, 64
Korchagin V. I., Girard T. M., Borkova T. V., Dinescu D. I., van Altena W. F., 2003, AJ, 126, 2896
Kruijssen J. M. D., 2012, MNRAS, 426, 3008
Kruijssen J. M. D., Maschberger T., Moeckel N., Clarke C. J., Bastian N., Bonnell I. A., 2012, MNRAS, 419, 841
Kupper A. H. W., Maschberger T., Kroupa P., Baumgardt H., 2011, MNRAS, 417, 2300
Lada C. J., Lada E. A., 2003, ARA&A, 41, 57
Lada C. J., Margulis M., Dearborn D., 1984, ApJ, 285, 141
Larson R. B., 1981, MNRAS, 194, 809
Maschberger T., 2013, MNRAS, 429, 1725
Maschberger T., Clarke C. J., 2011, MNRAS, 416, 541
Metchev S. A., Hillenbrand L. A., 2009, ApJS, 181, 62
Moeckel N., Bonnell I. A., 2009a, MNRAS, 396, 1864
Moeckel N., Bonnell I. A., 2009b, MNRAS, 400, 657
Moeckel N., Clarke C. J., 2011, MNRAS, 410, 2799
Moeckel N., Holland C., Clarke C. J., Bonnell I. A., 2012, MNRAS, 425, 450
Moyano Loyola G. R. I., Hurley J. R., 2013, MNRAS, 434, 2509
Offner S. S. R., Hansen C. E., Krumholz M. R., 2009, ApJ, 704, L124
Olczak C., Spurzem R., Henning T., 2011, A&A, 532, 119

Pang X., Grebel E. K., Allison R. J., Goodwin S. P., Altmann M., Harbeck D., Moffat A. F. J., Drissen L., 2013, ApJ, 764, 73
Parker R. J., Dale J. E., 2013, MNRAS, 432, 986
Parker R. J., Goodwin S. P., 2012, MNRAS, 424, 272
Parker R. J., Meyer M. R., 2012, MNRAS, 427, 637
Parker R. J., Bouvier J., Goodwin S. P., Moraux E., Allison R. J., Guieu S., Güdel M., 2011, MNRAS, 412, 2489
Parker R. J., Maschberger T., Alves de Oliveira C., 2012, MNRAS, 426, 3079
Parmentier G., Pfalzner S., 2013, A&A, 549, A132
Pelupessy F. I., Portegies Zwart S., 2012, MNRAS, 420, 1503
Portegies Zwart S. F., Makino J., McMillan S. L. W., Hut P., 1999, A&A, 348, 117
Portegies Zwart S. F., McMillan S. L. W., Hut P., Makino J., 2001, MNRAS, 321, 199
Prim R. C., 1957, Bell Syst. Tech. J., 36, 1389
Randich S., 2012, Chemical Evolution of the Milky Way, available at: http://www.sexten-cfa.eu/it/conferenze/conferences2012/details/17-Chem_evo_milky_way
Reggiani M. M., Meyer M. R., 2011, ApJ, 738, 60
Reggiani M. M., Meyer M. R., 2013, A&A, 553, A124
Rochau B., Brandner W., Stolte A., Gennaro M., Gouliermis D., Da Rio N., Dzyurkevich N., Henning T., 2010, ApJ, 716, L90
Sabbi E. et al., 2008, AJ, 135, 173
Salpeter E. E., 1955, ApJ, 121, 161
Sana H., Momany Y., Gieles M., Carraro G., Beletsky Y., Ivanov V. D., De Silva G., James G., 2010, A&A, 515, A26
Sánchez N., Alfaro E. J., 2009, ApJ, 696, 2086
Scally A., Clarke C., 2002, MNRAS, 334, 156
Schmeja S., 2011, Astron. Nachr., 332, 172
Schmeja S., Klessen R. S., 2006, A&A, 449, 151
Smith R., Fellhauer M., Goodwin S., Assmann P., 2011, MNRAS, 414, 3036
Spitzer L., Jr, 1969, ApJ, 158, L139
Steenbrugge K. C., de Bruijne J. H. J., Hoogerwerf R., de Zeeuw P. T., 2003, A&A, 402, 587
Tutukov A. V., 1978, A&A, 70, 57
Whitworth A., 1979, MNRAS, 186, 59
Wright N. J., Drake J. J., Drew J. E., Vink J. S., 2010, ApJ, 713, 871
Wright N. J., Parker R. J., Goodwin S. P., Drake J. J., 2014, MNRAS, 438, 639
Yu J., de Grijs R., Chen L., 2011, ApJ, 732, 16
Zasowski G. et al., 2013, AJ, 146, 81
Zinnecker H., 1982, Ann. New York Acad. Sci., 395, 226

This paper has been typeset from a TEX/LATEX file prepared by the author.